Cretaceous Research 148 (2023) 105535

Contents lists available at ScienceDirect

Cretaceous Research

journal homepage: www.elsevier.com/locate/CretRes

Late Barremian–Aptian paleoenvironmental variations and OAE1a environmental effect in the eastern Crimea

Maria Karpuk [a, *], Ekaterina Shcherbinina [a], Elena Shchepetova [a], Larisa Glinskikh [b], Galina Aleksandrova [a], Elena Kozlova [c], Boris Pokrovsky [a], Irina Latysheva [a, d], Ekaterina Brovina

[a] Geological Institute of RAS, Pyzhevsky Lane 7, Bld. 1, Moscow, 119017, Russia
[b] Trofimuk Institute of Petroleum Geology and Geophysics, Siberian Branch, Russian Academy of Sciences, Ac. Koptyug Ave., 3, Novosibirsk, 630090, Russia
[c] Center for Hydrocarbon Recovery, Skolkovo Institute of Science and Technology, Bolshoy Boulevard 30, Bld. 1, Moscow, 121205, Russia
[d] Moscow State University, Geological Department, Vorobiovy Gory 1, Moscow, 123103, Russia

ARTICLE INFO

Article history:
Received 1 December 2022
Received in revised form
22 February 2023
Accepted in revised form 7 March 2023
Available online 22 March 2023

Keywords:
Lower Cretaceous
NE Peri-Tethys
Foraminifera
Lithology
Ostracods
Calcareous Nannofossils
Palynomorphs
Stable isotopes
Climate reconstruction

ABSTRACT

The early Aptian Oceanic Anoxic Event 1a (OAE1a, or Selli Event) is widely known from many oceanic and inland sections as an interval of enhanced accumulation of sediments rich in total organic carbon (TOC), associated with the turnover in the global carbon budget and dramatic biotic variations. Our multidisciplinary study of the upper Barremian to lower upper Aptian deposits from the eastern part of Crimean Peninsula allowed us to confirm the presence of a layer that correlates to OAE1a and revealed significant reorganization in the planktonic and benthic foraminifera, nannofossils, ostracod and terrestrial plant communities at this level. The low-calcareous OAE1a deposits from the eastern Crimea lack in TOC that is not typical sedimentological response to this critical event. The OAE1a onset was associated with a nannoconid crisis, occurrence of low-abundance *Hedbergella* planktonic foraminifera, increased abundance of benthic foraminifera and ostracods and the bloom of *Classopolis* on the adjacent land. The calcareous microplankton biota was highly oppressed during OAE1a up to total elimination in the core of the event. Benthic assemblages indicate the occurrence of dysoxic conditions at the sea-floor. The absence of organic matter in the deposits of the OAE1a interval points to the low basinal biotic productivity and low input of terrestrial organic matter. We suggest that oligotrophication of the basin was related to the transgressive pulse, which led to small-scale landward moving of the coastal line barriered by coastal highland. The hot arid climatic conditions indicated by terrestrial plants, prevented the supply of nutrients and terrestrial organic matter into the basin that caused low algal and bacterial productivity and prevented accumulation of TOC-rich sediments. The termination of OAE1a coincides with the occurrence of warm humid climate and erosion of ephemeral coastal highland, more likely, built up by soft clayey sediments. The transit restoration of the normal marine biota in the early late Aptian was interrupted in the middle late Aptian by new long-lived regression led to enhanced terrestrial runoff and, possibly, fresh water input killed marine biota and caused the accumulation of low-calcareous clay.

1. Introduction

The mid-Cretaceous (Aptian to Turonian, ~126–90 Ma) is known as a time of greenhouse world, suggesting exceptionally warm climate (Hallam, 1985; Norris et al., 2002; Takashima et al., 2006; Friedrich et al., 2012; O'Brien et al., 2017; Bottini and Erba, 2018; O'Connor et al., 2019) and low equator-to-pole temperature gradient (Barron, 1983; Huber et al., 1995; Jenkyns et al., 2004; Pagani et al., 2014), which caused sluggish oceanic circulation and related periodically occurred oxygen deficiency in the bottom and intermediate waters. These climatic and hydrological changes led to worldwide accumulation of sediments rich in organic matter (Schlanger and Jenkyns, 1976; Jenkyns, 1980; Bralower et al., 1994; Pancost et al., 2004). The short-lived (<1 Ma) episodes of increased sequestration of organic matter in the oceanic basins, associated with climatic warming, perturbations in carbon cycle, variations in

* Corresponding author.
E-mail address: maria.s.karpuk@gmail.com (M. Karpuk).

https://doi.org/10.1016/j.cretres.2023.105535
0195-6671/

marine biota, including increased rate of evolution of micro- and nannoplankton and enhanced algal and phytoplankton productivity (Bralower et al., 1993; Menegatti et al., 1998; Luciani et al., 2001; Leckie et al., 2002; Jenkyns, 2003; Dumitrescu and Brassel, 2006; Bottini et al., 2012; Föllmi, 2012; Trabucho-Alexandre et al., 2012) are designated as Oceanic Anoxic Events (OAEs, Schlanger and Jenkyns, 1976).

One of the most impressive OAEs is the early late Aptian OAE1a or Selli Event (120 Ma), which is detected in many oceanic, hemipelagic and shelf settings. It is characterized by wide black-shale accumulation, negative $\delta^{13}C$ excursion at the OAE1a onset followed by prominent positive $\delta^{13}C$ excursion, sea-level variations, oceanic crust production, perturbation in marine nanno- and microplankton communities and reorganization of terrestrial flora (Erba, 1994; Heimhofer et al., 2006; Heldt et al., 2012; Quijano et al., 2012; Bottini et al., 2015; Erba et al., 2015; Patruno et al., 2015; Lubke and Mutterlose, 2016; Naafs and Pancost, 2016; Fu et al., 2020; Deconinck et al., 2021 a.o.). In the NE Peri-Tethys, the repercussions of OAE1a occur in a shallow epicontinental basin of the Russian Plate, where they are represented by TOC-rich black shales (Gavrilov et al., 2002; Zakharov et al., 2013; Zorina, 2014; Rogov et al., 2019).

The upper Barremian–Aptian deposits are widespread in the southern Crimea extending in the roughly W—E direction. They are composed of soft gray to pale calcareous mudstones and marls mostly lack in macrofossils, but rich in planktonic and benthic foraminifera, nannofossils, dinocysts and ostracods. The studies of microfossil assemblages from the southwest and central Crimea enabled the detailed stratigraphic division and correlation of these deposits (Gorbachik and Yanin, 1972; Gorbachik, 1986; Baraboshkin et al., 2004; Karpuk and Tesakova, 2013, 2014; Matveev, 2016; Brovina, 2017; Brovina et al., 2017; Karpuk et al., 2018). However, despite a wide cropping-out of the upper Barremian–Aptian strata, the interval correlatable to OAE1a appeared to be covered by vegetation in the most parts of the area. In the southeast Crimea, Barremian—Aptian deposits are incorporated in the Taygan Formation (Astakhova et al., 1984; Gozhik, 2013; Anfimova, 2015). The continuous exposure of this Formation named Zavodskaya Balka (ZB) is located in the vicinity of the city of Feodosia (Fig. 1A, B). Our previous research (Karpuk et al., 2018) allowed the recognition of the OAE1a interval in ZB section that provides a perfect opportunity to study biotic, sedimentological and geochemical aspects of this critical event in the wide Crimea—Caucasian Basin.

In the early Cretaceous, the area of the city of Feodosia was located in the outer shelf of the NE Peri-Tethys near the bend of the slope of Sudak Trough (Fig. 1D), which was formed in the Jurassic and underwent folding at the Eocene/Oligocene transition (Nikishin et al., 2015a, 2015b). Structurally, this region belongs to the Feodosian block of eastern Crimea Folded Monocline (Fig. 1D) forming the eastern closure of the Crimean Meganticlinorium. This area is characterized by significant variations in facies composition and thickness of the Lower Cretaceous deposits (Filatov, 1961; Muratov, 1973). The exposed thickness of the Taygan Fm. in the stratotype area is ca.500 m (Astakhova et al., 1984), whereas it barely reaches 40 m in the studied section. The Taygan Fm. onlaps the lower Hauterivian sands and sandstones of the Mazanka Fm (Muratov, 1973) and is conformably covered by the lower Albian Kurskoe Fm. (Gozhik, 2013; Anfimova, 2015), which is built up by alternated mudstones and sandstones. In the Barremian to early Aptian, a wide land of the East-European Platform was located closely northward from the Crimea (Baraboshkin, 2005), providing the supply of clastic material into the basin.

The recent integrated microfossil (calcareous nannofossils, planktonic and benthic foraminifera, ostracoda, palynomorphs) and paleomagnetic study of ZB section delineated the stratigraphic range of the succession exposed as the uppermost Barremian to upper Aptian, provided a detailed biozonal division according to different microfossil groups and defined the interval correlated to the OAE1a (Karpuk et al., 2018). This work is aimed to the paleoecological reconstructions of the late Barremian to late Aptian time interval, with special focus on the paleoenvironmental changes in this part of the Crimea—Caucasus Basin during OAE1a.

2. Material and methods

2.1. Material

The outcrop ZB was studied and sampled in the upper SE part of the ravine crossing the eastern wall of the abandoned quarry located 1 km west from the city of Feodosia, on the left from the road Feodosia—Ordzhonikidze (GPS data N 45°1′56″ E 35°20′14″) (see Fig. 1B). The 33 m-thick outcrop of the mid-Cretaceous marine mudrock (claystone to mudstone) succession contains numerous irregular intercalations of decimeter-scale compact carbonate beds (Fig. 2). This succession was initially sampled with equal intervals (23 samples) and later few additional samples were taken from the intervals, which were suggested to be correspondent to the OAE1a. Besides, few additional samples (21a, 15a, 13a, 2a) were collected from carbonate intercalations.

2.2. Methods

All samples collected were processed for micropaleontological, microfacies and geochemical analyses using responding methods in the laboratories of the Geological Institute of the Russian Academy of Sciences, Moscow and TOC content was measured in the Laboratory of Center for Hydrocarbon Recovery, Skoltech, Moscow.

Sedimentological studies. To identify sediment granulometry, fabric and rock-forming minerals, samples were examined under petrographic microscope AXIO LAB.A1 Pol, Carl Zeiss. Standard petrographic thin sections were prepared from the main 23 samples (22, 21, 19, 17—13, 11—2) and 5 additional (1501—1505), taken at the interval corresponding to the OAE1a; four extra samples of nodular carbonate beds from the different levels of the section were also analyzed. Grain size of the mudrock (samples 1—23) was measured using Analysette 22 MicroTec Plus laser diffraction analyzer, equipped by wet dispersion unit and ultrasonic box. Five measurements were performed for each sample (precision ±10%) and median particle size (volume-weighted), sorting and skewness coefficients were calculated.

Clay minerals were defined by X-ray diffractometry (XRD) of the oriented samples. The clay fraction (<2 μm), yielded by sedimentation method, was precipitated onto glass slides to provide a specimen 34 × 17 mm in size (Moore and Reynolds, 1997). XRD-patterns were recorded in three states (dry air, ethylene glycol solvated and heated to 550 °C) using a D8 Advance Bruker (radiation: CuKα, 40кВ, 40 мА). The main clay minerals are illite and kaolinite. Chlorite, chlorite—smectite and illite-smectite mixed layered minerals are detected sporadically as trace amounts.

To estimate the kaolinite-illite ratio, which is widely applied as paleoclimatic proxy, the clay fraction of six representative samples (23, 19, 13, 9, 5, 2) was treated with 10% HCl and then heated to 350 °C, as the presence of small quantities of chlorite, mixed layered chlorite—smectite and illite-smectite makes difficult the definition of the kaolinite contribution due to overlapping peaks in XRD patterns. X-ray images for these specimens were recorded at speed 2° 2θ per minute in the interval 2—32° 2θ and quantification was performed by simulation of the experimental diffractograms (Drits and Sakharov, 1976; Drits and Tchoubar, 1990; Sakharov and

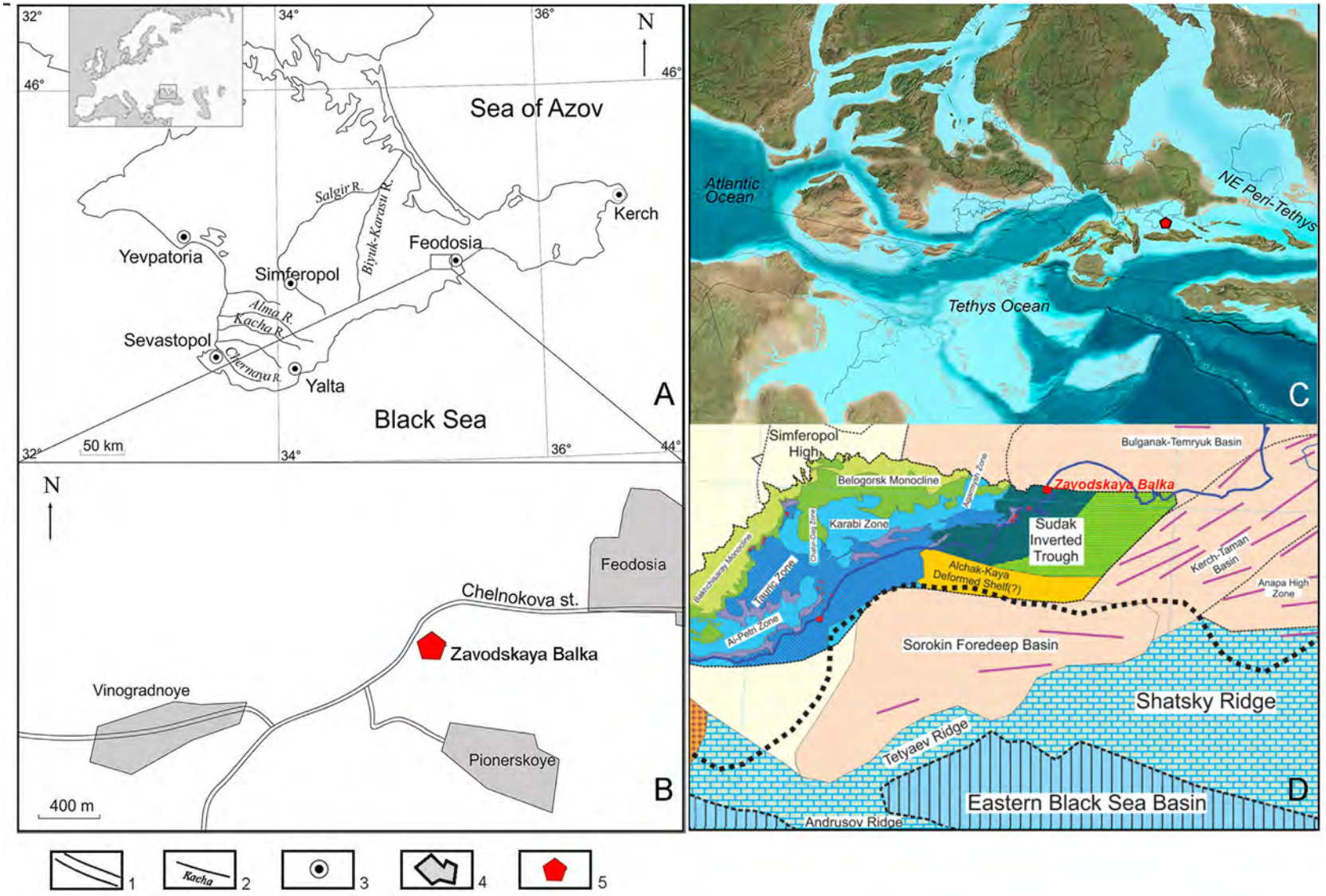

Fig. 1. Geographic position of Zavodskaya Balka (ZB) section (A, B), early Aptian paleogeography of Europe (C, modified from Deep Time Maps, http://deeptimemaps.com) and tectonic sketch-map of the eastern Crimea (D, modified from Nikishin et al., 2015b). Symbols: 1 — road, 2 — river, 3 — city, 4 — town, village, 5 — ZB outcrop.

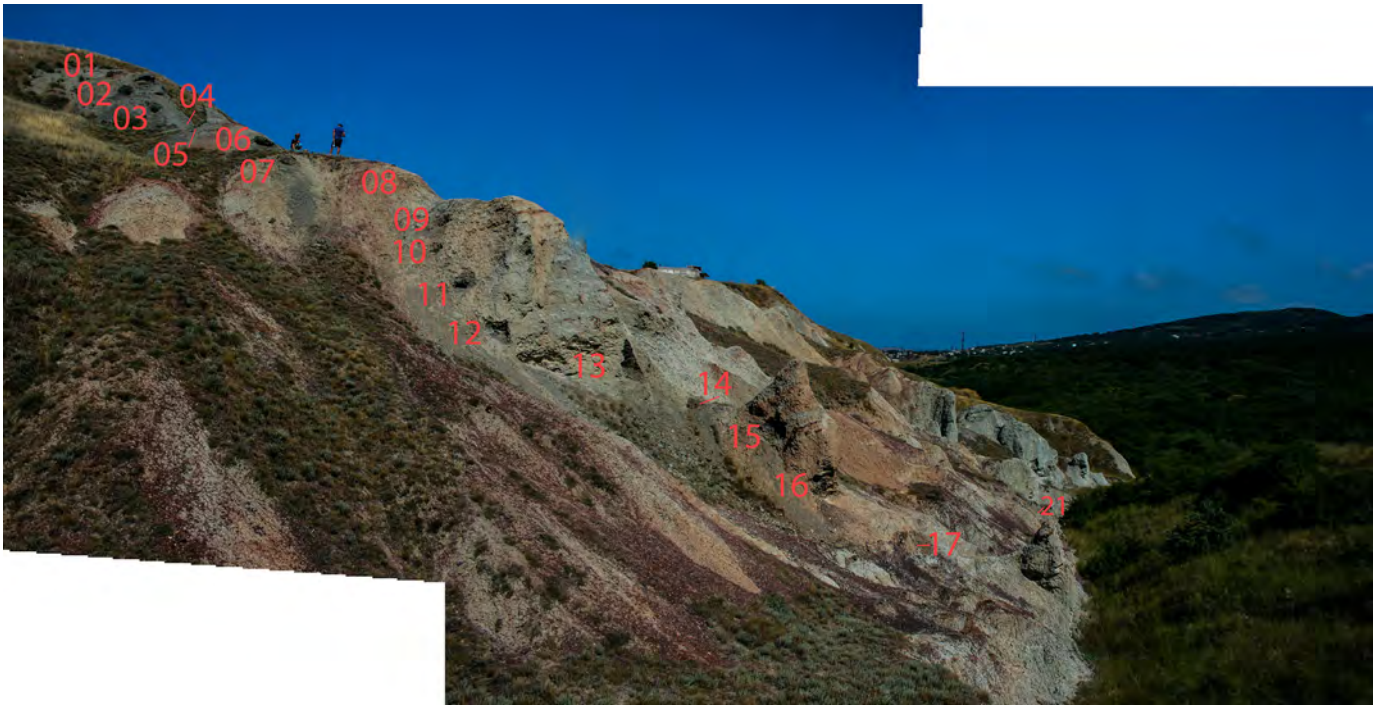

Fig. 2. Outcrop of ZB section in the vicinity of the town of Feodosia. Numbers are samples collected.

Lanson, 2013) using a model assuming the specimens as a physical mixture of kaolinite and illite.

To measure the values of the carbonate minerals the insoluble residue test was applied using the dissolution of 4–10 g of clay rocks (28 samples) in 20–40 ml of 2 M HCL (Briggs, 1977; Cogley and Aikman, 1997) (Table A.1). The reproducibility of measurements is ±0.5%. More precise diagnostics of carbonates (calcite, siderite) and other authigenic minerals (apatite, pyrite, goethite) were carried out petrographically, by XRD analysis of rock powders and studies of their morphologies and chemical compositions under scanning electron microscope (SEM) CamScanMV-2300 with the Oxford Inca Energy 200 EDS system.

The TOC (total organic carbon, wt. %) content was measured using HAWK Resource Workstation (Wildcat Technology) in the 27 samples according to standard procedures for Rock-Eval pyrolysis (Espitalié and Bordenave, 1993; Tissot and Welte, 1984). S1, S2, S3 and T_{max} (°C) were measured (Table A.2). Parameter S1 demonstrates the amount of free hydrocarbons (HC) in each sample (mg HC/g rock). S2 is a product of thermal cracking of kerogen and characterizes residual hydrocarbon generation potential (mg HC/g rock). S3 is the organic carbon dioxide yield produced by kerogen during pyrolysis (mg CO_2/g rock). TOC content, hydrogen index (HI = S2/TOC × 100), oxygen index (OI = S3/TOC × 100) and production index (PI = S1/(S1 + S2) were calculated from the values obtained.

Stable isotope analysis. The carbon and oxygen isotope analyses were made from the bulk carbonate and the shells of *Dentalina* spp. benthic foraminifera. Powdered sediment was processed with 100% phosphoric acid at 50 °C using Gasbench II connected to Thermo Electron Delta V Advantage mass spectrometer. The values obtained are given in per mille relative to V-PDB by assigning $\delta^{13}C_{carb}$ value of 1.95‰ and a $\delta^{18}O_{carb}$ value of 2.20‰ to NBS19. The reproducibility of the determination of $\delta^{18}O$ and $\delta^{13}C$ in laboratory standards is ±0.1‰.

Foraminifera and ostracods. The sample preparation evolved from the technique described by Sohn (1961). Each sample of clay was dessicated and approximately 500 g were boiled with sodium bicarbonate, washed over 0.1 mm sieve and dried at 25 °C. All ostracod and benthic foraminifera (BF) specimens from the 0.1–1 mm fraction were picked. Ostracods were collected under light microscope Bresser Advance and BF under light microscope Carl Zeiss Stemi 2000-C.

Calcareous nannofossils. The smear-slides for nannofossil study were prepared from the raw sediment of all collected samples with Norland Optical Adhesive 61 using standard techniques (Bown and Young, 1998). Nannofossils were examined at 1250× magnification under light microscope Olympus BX41. The total abundance of selected taxa was estimated on the basis of a count of 300 specimens per smear-slide from the variable number of fields of view in the randomly distributed transverses. The variations in the total nannofossil abundance are expressed as the changes in the average nannofossil abundance per field of view counted from 50 random fields of view.

Palynomorphs were studied from 12 samples (23, 19, 17, 15, 14, 13, 1504, 10, 8, 6, 3, 1). Chemical preparation of samples for palynological study followed the method developed by the research team of the Geological Institute of the RAS (see, for example, Shcherbinina et al., 2016). Spores, pollen and microphytoplankton (dinoflagellates, algae) were examined at 400–600× magnification under a light microscope Carl Zeiss Axioplan and their pictures were made using a Canon PowerShot A640 camera and Axiovision visualization programme. Two hundred specimens were counted from samples with abundant palynomophs and all specimens from the samples with rarer palynomophs.

3. Results and interpretation

3.1. Lithology

3.1.1. Results

The studied Barremian–Aptian sequence consists of rather uniform light gray mudrocks varying from bluish carbonaceous

mudstones to greenish claystones. Lithology does not vary significantly through the section, any erosional contacts or distinct boundary surfaces were not recognized. The diagenetic carbonate nodules and nodular beds (ca. 0.1–0.2 m thick) occur at the isolated levels; they are clearly visible in the outcrop due to their reddish-brown color caused by supergenically formed iron oxides.

The primary bedding and/or lamination are completely destroyed by bioturbation in the mudrocks. Only mottling ichnofabric can be observed in the wet polished rock slices and petrographic thin sections. The rare indistinctly outlined burrows (*Chondrites, Planolites, Phycosiphon, Ryzocorallium*?) can be recognized. This suggests a slow accumulation of clayey sediment and signifies mostly normal oxygenation of the bottom and pore waters.

The results of the laser diffraction indicate that all samples are clay (particle median size 3.1–3.6 μm) with very low proportion of silt- and sand-sized graines (>4 μm). This grain size persists across the whole succession. However, a general coarsening-upward trend is recognized from the upper Barremian–lower Aptian to the upper Aptian deposits by the increase in the average particle size (Fig. 3). It is noteworthy that grain coarsening occurs in the uppermost lower Aptian to upper Aptian deposits, while the lower part of the section (samples 23–17) is characterized by the lower average particle size.

The petrographic observations demonstrated the variations in the concentrations of terrigenous silt grains in the claystones from 1–2% to 5–10% with rare increase up to 10–20% in the upper Barremian–lower Aptian interval. However, despite the lower amount of silt admixture in the upper part of the studied section, the median particle size slightly enlarges up the section: from 10 to 50 μm in the upper Barremian and the lower part of the lower Aptian (samples 23–17) to 50–100 μm in the upper part of the lower Aptian and upper Aptian (samples 14–1). The admixture of fine sand grains (0.1–0.2 mm) is contained in the mudrocks at the particular levels (samples 13, 14).

Two types of silt and fine sand material are observed in the mudrocks: 1) highly mature, represented by quartz grains and flakes of colorless and bluish-green hydrated micas, sometimes angular fragments of semi-allochtonous glauconite, transported from the neighbor facial zones, and 2) relatively immature, presented mainly by rather coarse (up to 0.1–0.2 mm) flakes of greenish-brown biotite, rare grains of acid plagioclase and, rarely, fragments of weakly altered felsic volcanic rocks. At peculiar intervals (samples 18–13), rounded (0.25–0.5 mm to 1 cm in diameter) accumulations of finely dispersed authigenic glauconite occur in the clays. These glauconite concentrations, probably, were formed during the periods of lower sediment supply (Odin, 1988; Amorosi, 1995, 2013; Föllmi, 2016; Tribovillard et al., 2023).

3.1.1.1. Carbonate material. Carbonate material in the claystones is mainly of biogenic origin. It is represented by calcareous nannofossils (CN), planktonic foraminifera (PF) tests and their fragments. The calcareous benthic bioclasts include echinoid spine debris, tests of benthic foraminifera (BF) and ostracoda valves. Besides the calcareous bioclasts, few pieces of tiny siliceous sponge spicules and rare small phosphatized fish detritus occur.

Biogenic carbonate material is spread unevenly along the section showing higher concentrations (≥20% $CaCO_3$) in the upper Barremian to the lower part of the lower Aptian (samples 23–17, Fig. 3) and in the lower part of the upper Aptian (samples 1503–7). The high amount of biogenic carbonate in the lower interval is caused by high CN abundance, while in the higher interval it is formed by both CN and PF. The low-calcareous clays (<10% $CaCO_3$), almost lacking in the planktonic carbonate material, occur in the uppermost part of the lower Aptian in the short stratigraphic interval corresponding to OAE1a (samples 14–13) and in the upper part of the upper Aptian (samples 4–1).

3.1.1.2. TOC content and OM-lithofacies. In the studied mudrocks, the TOC values are rather low (0.3 ÷ 0.8 wt %) (see Fig 3). Kerogen assemblages are dominated by terrestrial phytoclasts (70–99 vol. %) with scarce reworked coal fragments (<0.1 mm) and low-abundance terrestrial palynomorphs (spores and pollen). Marine and freshwater palynomorphs, as well as amorphous organic matter (AOM), are present within peculiar stratigraphical intervals.

Three types of palynofacies or kerogen assemblages (P1, P2 and P3) can be recognized through the section (Fig. 4). P1 (Fig. 4A) (samples 23–17) is mainly composed of phytoclasts (90–95 vol. %) with small amount of terrestrial palynomorphs (spores and pollen) and scarce dinoflagellate cysts. P2 (Fig. 4B) (samples 16–8) exhibits an increase (up to 20 vol. %) in the terrestrial palynomorphs, and P3 (Fig. 4D) (samples 7–1) consists almost entirely of none-opaque (oxidized) phytoclasts (98–99 vol. %) with scarce terrestrial palynomorphs and freshwater algae (*Acrytarch, Botryococcus*), which are abundant at the level of sample 3. P2 palynofacies is identified in the lower Aptian deposits. The narrow interval (samples 13–14) of none-calcareous clay, characterized by regular presence of AOM particles (5–20 vol. %) in the kerogen assemblage (see Fig. 4C), corresponds to the OAE1a (Karpuk et al., 2018). The inversed correlation of HI and OI graphs at this level (see Fig. 3) shows the increase of marine OM along with the decreased oxidation of buried OM.

The low TOC values do not allow the estimation of the proportion between TOC and carbonate carbon or carbonate material. There is an implicit inverse relation between them, which is more evident in the uppermost part of the section (sample 6–2). However, the highest measured TOC content (0.8 wt %) (avg 0.7 in the interval 26–32 m, samples 2–6) occurs in the uppermost part of the section (sample 2) in the non-calcareous mudstone with kerogen assemblage, which is almost totally consists of phytoclasts. The lowest TOC and $CaCO_3$ values are detected in sample 13.

Low TOC values in the mudrocks are accompanied by poor hydrocarbon yield (S1 < 0.234, the average 0.8 mg HC/g rock, S2 < 0.41, the average 0.40 mg HC/g rock) (see Fig. 3). The highest S2 value of 0.41 mg HC/g rock is registered in the sample 14 collected from the non-calcareous clay in the interval corresponding to the OAE1a, which is featured by occurrence of AOM particles.

3.1.1.3. Clay mineralogy. According to XRD results, clay minerals in the mudrocks of the upper Barremian to uppermost Aptian mainly comprise the kaolinite and illite with minor amount of chlorite and very low portion of chlorite–smectite and illite-smectite mixed layered minerals, where smectite layers dominate.

Kaolinite/illite ratio shows an upward increase in the relative abundance of kaolinite from 9–11% to 27–30%, as calculated by simulation of experimental XRD-patterns (Fig. 2). Thus, illite predominates in the studied claystones. Kaolinite is present in small amounts in the clay fraction of rocks of the upper Barremian–lowest Aptian interval (samples 23–14) (Fig. 5). This ratio persists up to the lower/upper Aptian boundary, where the portion of kaolinite increases distinctly at the level of the sample 13. Then kaolinite increases progressively in the upper Aptian claystones (samples 13–9), and in the uppermost part of the section (samples 5–2), the clay mineral association contains permanently higher (i.e. 2.5–3 times) amount of kaolinite than is observed in the Barremian deposits at the base of the studied section.

3.1.1.4. Microstructures of the soft-sediment deformation in mudrocks. Microstructures of the soft-sediment deformation were

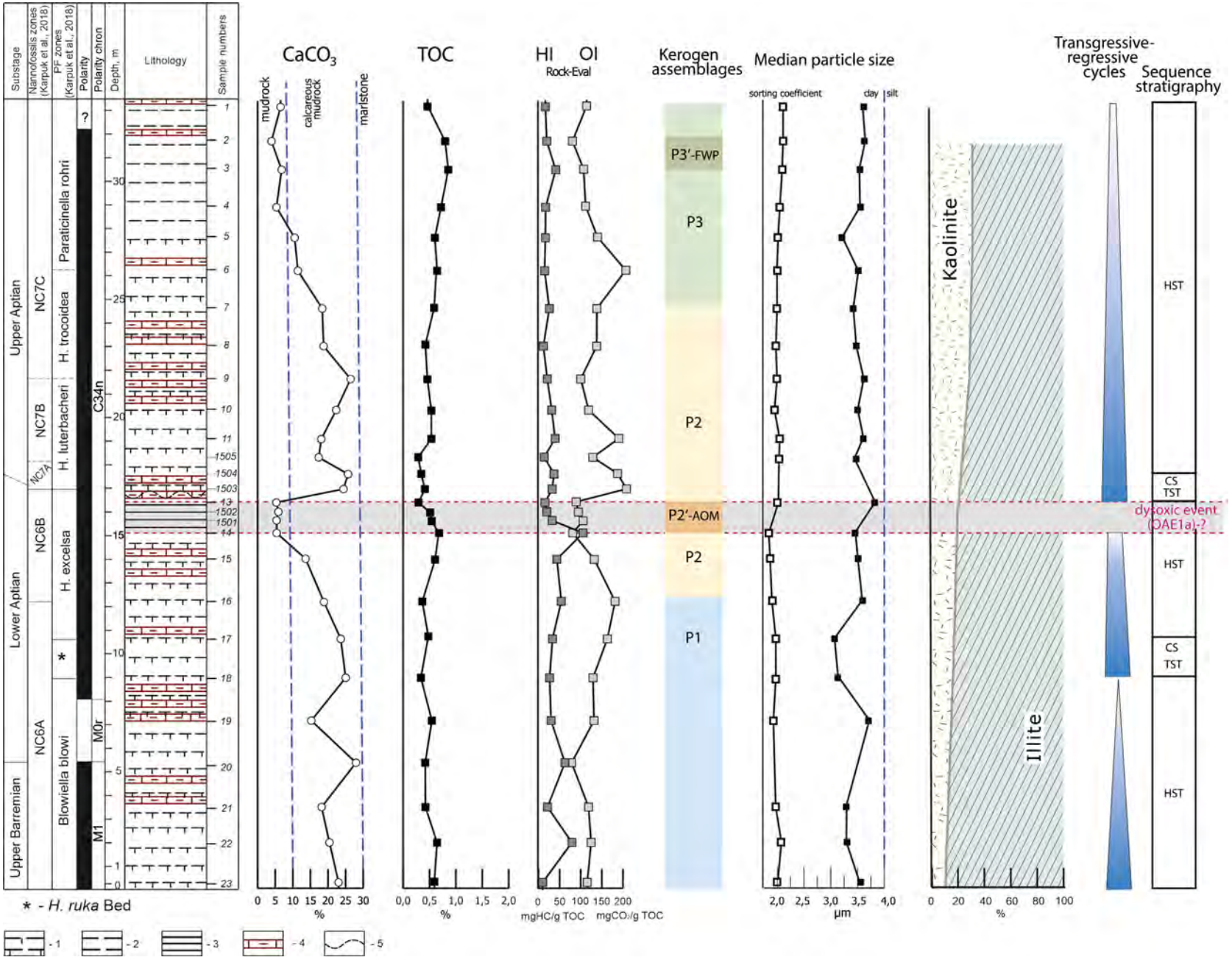

Fig. 3. Lithology, carbonate and TOC contents, pyrolitic HI, OI indices, kerogen assemblages, granulometric characteristics, clay mineral composition, transgressive-regressive cycles and sequence stratigraphy of the ZB section. FWP – freshwater palynomrphs, AOM – amorphous organic matter, HST – highstand system tract, TST – transgressive systems tract, CS – condensed section, P1, P2 and P3 – kerogen assemblages (see text for explanation). Symbols: 1 – calcareous mudstones, 2 – low calcareous mudstones, 3 – clays of the OAE1a interval, 4 – diagenetic concretions of limestones and marlstones, 5 – depositional break.

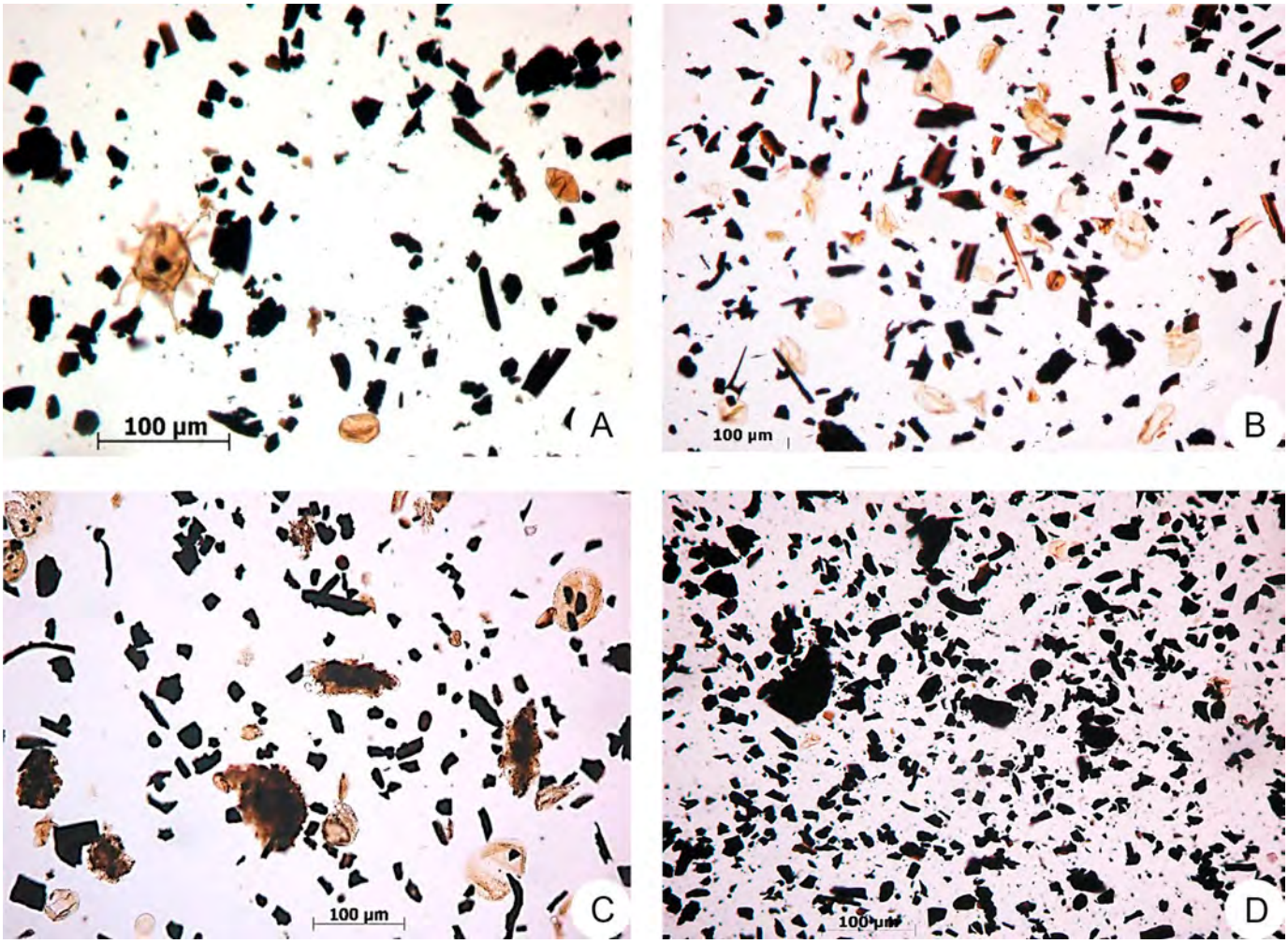

Fig. 4. Kerogen assemblages of the upper Barremian–Aptian mudrocks: A – palynofacies type P1 (uppermost Barremian, sample 23) consists of phytoclasts (90–95 vol %), terrestrial (2–5 vol %) and marine (dynoflagellate cysts) palynomorphs (2–5 vol %); B – palynofacies type P2 (lower Aptian, sample 15) consists of phytoclasts (70–75 vol %) and terrestrial palynomorphs (25–30 vol %); C – palynofacies type P2′-AOM (lower Aptian, sample 13) consists of phytoclasts (60 vol %), terrestrial palynomorphs (20 vol %) and amorphous OM (20%); D – palynofacies type P3′-FWP consists of phytoclasts (95–99 vol %), terrestrial palynomorph debris (1–5 vol %) and scarce freshwater palynomorphs.

studied in the middle part of the section, presumably corresponding to OAE1a and surrounding samples 14, 1501, 1502, 13, 1503, 1504, and 1505. Non-deformed bioturbation (sample 1505, Fig. 6B) and microstructures of the soft-sediment deformation were observed in the mudrock. Noteworthy are some peculiarities in the mudrock microstructures observed in the middle part of the section (samples 14, 1501, 1502, 13, 1505). The specific wavy-banded microstructures related with sliding thin beds of unconsolidated clay are observed in the thin-sections (sample 13). At the later epigenetic stages, some deformed beds were colored in reddish-brown by ferrum oxides, while other persisted to be pale (Fig. 6A).

The study of petrographic slides showed mudrock microstructure similar to foliation in shists, particularly exhibited by the occurrence of clusters of very small (0.01 mm or less) mica flakes with the same orientation. Such a foliation, probably, partially inherits primary depositional structure of muddy sediment. However, the diverse pattern showing mica flakes oriented differently in adjacent blocks is observed in the sample 13. In the sample 14, the intersected foliation surfaces with the preferred mica orientation divide the mudrock into small subangular blocks (Fig. 6B, C). This type of microstructure is, more likely, caused by early disintegration of weakly consolidated clayey sediment.

In other samples (14, 1501, 1502, 13, 1505; Fig. 6D), the microfoliation developes in two crossing directions. In these cases, the foliation is, possibly, derived from aggregated clay sediment, showing the signs of initial coagulation. Such a microstructure could be caused by the transformation of highly coagulated clay sediment with a highly porous structure and high water saturation into a more compact finely dispersed microstructure (Leeder, 1982).

3.1.2. Interpretation

3.1.2.1. Lithology. The granulometric characteristics of the sediment, ichnofabric pattern, high terrigenous/biogenic components ratio, domination of planktonic microfauna and occurrence of BF and ostracod shells enable us to designate the studied Barremian–Aptian mudrocks as hemipelagites accumulated in distal marine offshore at relatively shallow depths (no more than few hundreds of meters). The sediment accumulation was controlled by vertical settling of clay and silt particles. The slow lateral sediment transportation was likely generated by a river plume, which was the most probable sediment transporter in the basin during Aptian. This interpretation is supported by high abundance of the phytoclasts and terrestrial palynomorphs in the kerogen assemblages, as well as by the low TOC content and negligible hydrocarbon potential of the Barremian–Aptian mudrocks.

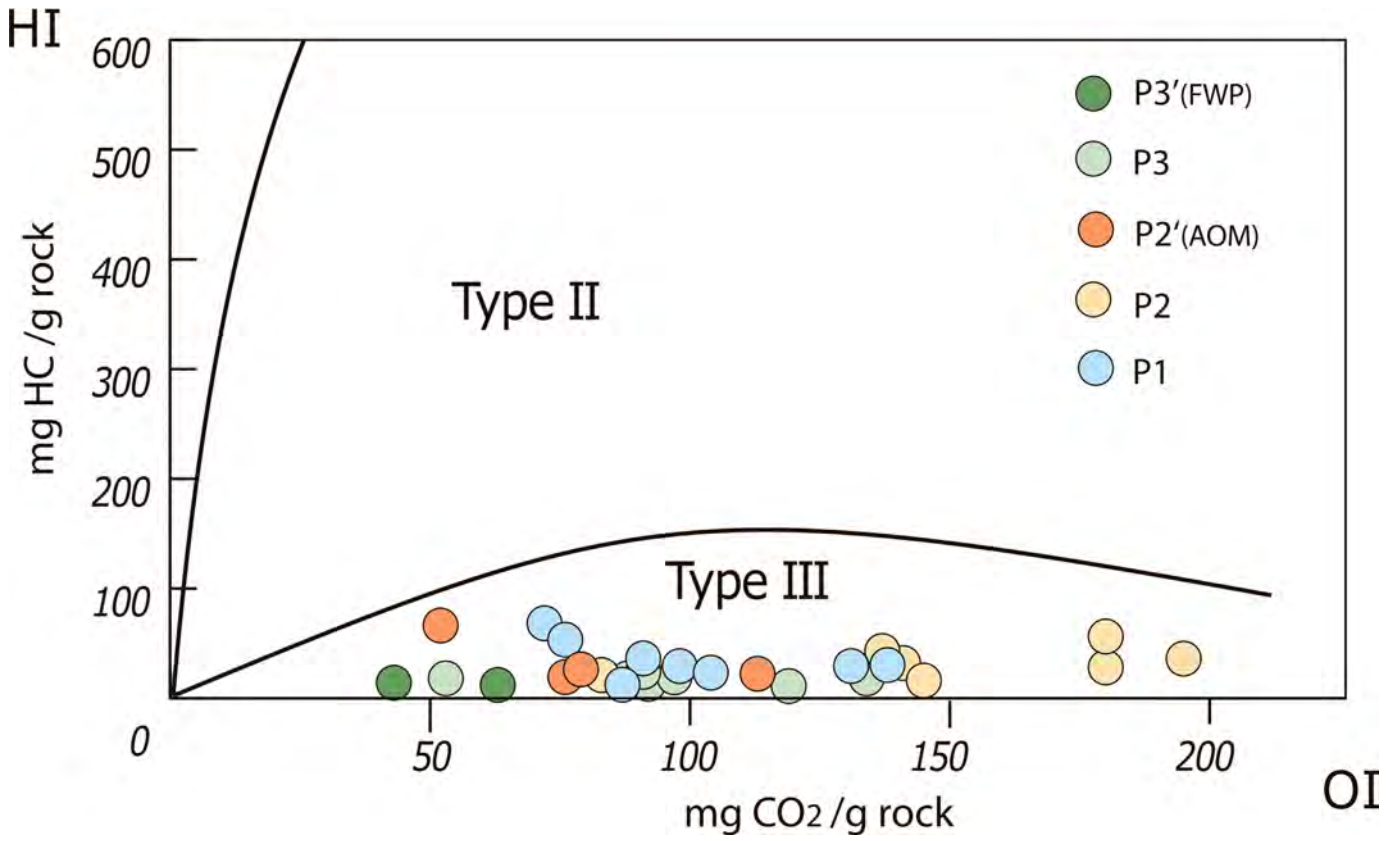

Fig. 5. Modified van Krevelen diagram of Hydrogen index (HI) versus Oxygen index (OI) showing kerogen quality of the studied samples (Espitalié et al., 1985).

3.1.2.2. TOC content. Such a poor hydrocarbon yield usually does not show a distinct peak on the most of pyrograms and this does not allow the precise definition of T_{max} for clayey sediments. Taken alone, a registration of the highest S2 gives unreliable range 374–486 °C. Therefore, the kerogen type has been defined using TOC—S2 plot (Langford and Blanc-Valleron, 1990; Tyson, 1995). All samples fall into the field of the type III kerogen (Fig. 5), which is assumed to be a kerogen of terrestrial origin. This is in a good agreement with palynofacies indications. The increase in the value of parameter S2 in the sample 14 (see Fig. 3) is consistent with an increase in the proportion of marine-derived amorphous OM in the kerogen of this claystone. The values of the highest temperature for hydrocarbon extraction, when possible, to define it correctly, indicate a low thermal maturity (411—436 °C) of the kerogen.

The obtained results show that the clayey sediments accumulated during OAE1a are not enriched in OM in the studied section. However, there is the indication of enhanced marine OM preservation at one of the levels of the lower Aptian (samples 13—14). This specific enrichment in the marine AOM of non-calcareous claystone within the narrow interval of the lower Aptian enables the suggestion of low-oxygen conditions at the bottom and/or pore waters during the clayey sediment accumulation.

3.1.2.3. Clay mineralogy. The low-ordered dioctahedral *illite* is considered mainly as a product of mechanical disintegration and a minor chemical degradation of trioctahedral micas under reduced water supply, featured for hot arid or cold conditions. The *kaolinite*, on the other hand, is an alumosilicate with simple chemical composition, which is usually considered as an end product of intensive chemical weathering and an indicator of warm humid climate. Besides, there are suggestions (Rateev, 1964; Gibbs, 1977; Deconinck et al., 2003; Godet et al., 2008; Zuo et al., 2019) that the precipitation of kaolinite from the terrigenous suspension can precede the precipitation of other clay minerals and accumulate relatively closer to shore line due to its relatively large, isometric particles less capable to the floating; however, this mechanism is still not studied in details. The Lower Cretaceous deposits of the studied succession are characterized by simple composition of clay mineral assemblage clay mineral assemblage, containing mainly illite and kaolinite with upsection increase of kaolinite percentage (see Fig. 3). This trend can be caused by increased climatic humidity and enhanced chemical weathering on the adjacent land. The kaolinite weathering crusts are widely distributed in the upper Aptian of the central part of the Ukrainian Shield and Black Sea Lowland (Voronova, 1984; Voronova and Yanovskaya, 1991; Gozhik, 2013) as well as in the middle Aptian (Gherghina Fm.) of Central and South Dobruja (Avram et al., 1988; Dragastan et al., 2014)

This interpretation can be supported by the revealed paleoecological signals (discussed below) of decreased salinity in the basin at the end of the late Aptian. The lowered salinity could be the result of more significant precipitation, enhanced land drainage and more active runoff of river and meteoric waters into the marine paleobasin. At the same time, the recognized trend can be the result of the shallowing of the basin and regression that can be evidenced by a simultaneous slight increase of the chlorite amount (see Fig. 7) in the clay mineral assemblage.

3.1.2.4. Microstructures of the soft-sediment deformation in mudrocks. A dramatic reorganization of the structural type of clayey sediment in the middle of the section (samples 14, 1501, 1502, 13, 1505) could be the result of local seismic or gravitational event that occurs during early burial stage of these clay

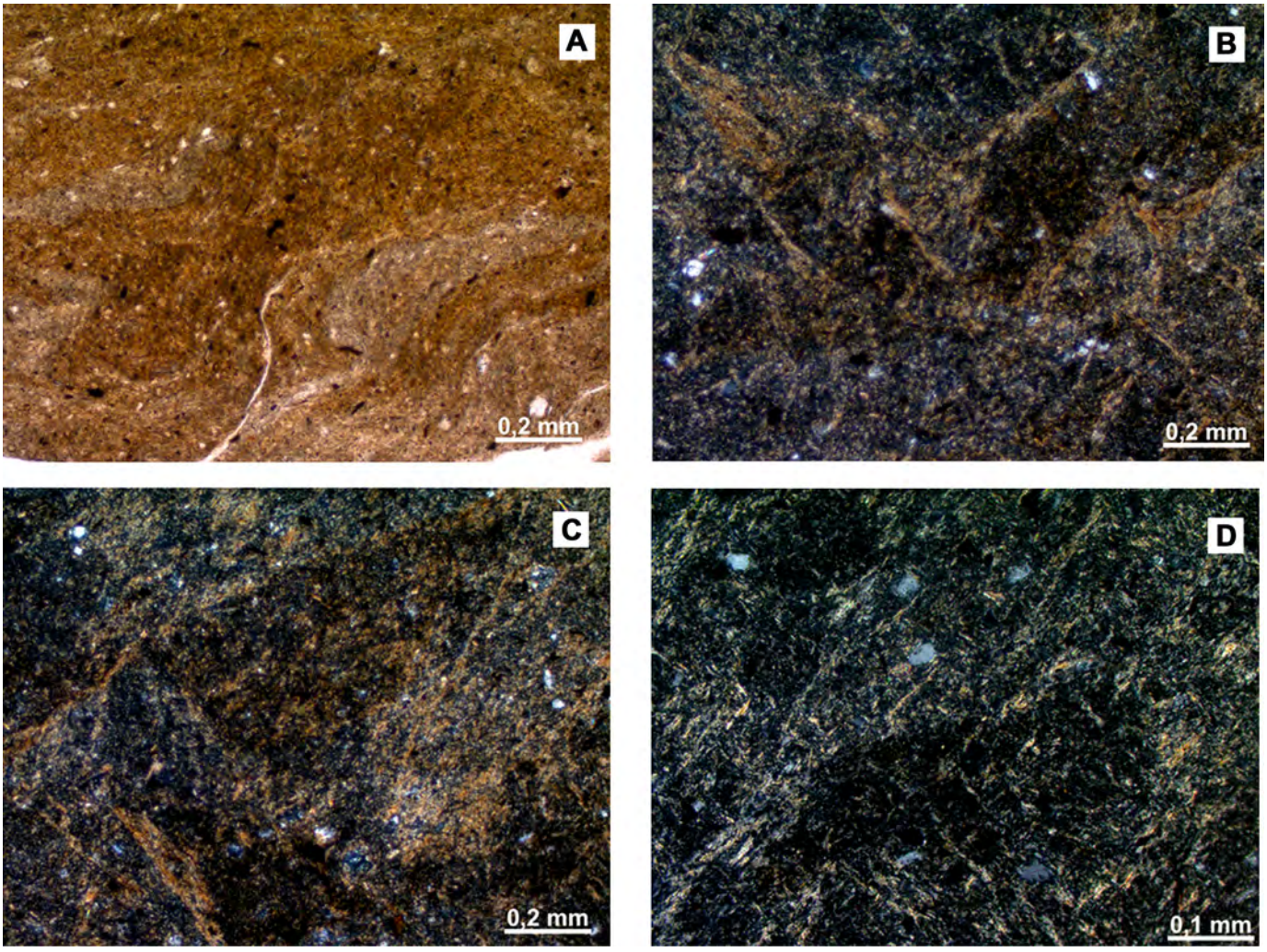

Fig. 6. Microphotographs of thin-sections showing the microstructures of the soft-sediment deformation in the mudrocks: A – wavy-banded microstructures related with rock sliding (sample 13); B, C – the intersected foliation surfaces divide the mudrock into small subangular blocks (sample 14); D – microfoliation oriented in two crossing directions (sample 1502).

accumulation. Thus, the mudrocks are weakly transformed during the epigenetic stages and their lithological structures were mainly formed during the sedimentation. Overall, in the interval corresponding to OAE1a possibly appeared seismic events which caused displacement of microfoliation and consedimentary slumping on local roughness of the basin bottom.

3.2. Benthic foraminifera

3.2.1. Results

Benthic foraminifera (BF) are of special importance as the direct indicators of physical and chemical characteristics of the bottom water and indirect markers of the water depth. BF communities are affected by multiple hydrological (temperature, salinity, water depth, nutrient availability, light intensity, turbidity, pH and the concentrations of oxygen and calcium carbonate) and ground (porosity, grain size, degree of solidification) characteristics. The depth of the foraminiferal habitat in the sediment depends mainly on the oxygen and nutrient availability. The epifaunal microhabitat is advantageous for taxa demanding nutrient and/or oxygen limitations, whereas environments with high organic carbon content in sediment are dominated by infaunal taxa (Tyszka, 1994; Van der Zwaan et al., 1999; Reolid et al., 2008, 2010; Nikitenko et al., 2013).

The studies of modern and ancient foraminiferal assemblages have shown that the morphology of the shell, mode of coiling, type of aperture and pore occurrence reflect the different life styles and feeding strategies (Nagy 1992; Tyszka, 1994; Reolid et al., 2008, 2010; Nikitenko et al., 2013; Colpaert et al., 2017). The use of morphological categories instead of taxonomic in the palaeoenvironmental interpretations seems to be more reasonable because: 1) the morphological approach allows the reliable comparisons of assemblages of different ages because it reduces the effect of taxonomic divergences caused by biological evolution and 2) taxonomical definitions at the species level are not required (Nagy, 1992). In our paleoenvironmental reconstructions, we use the morphological groups (MG), which are suggested to be corresponding to peculiar microhabitat depth within the sediment, recognized by authors mentioned above for Jurassic foraminiferal assemblages (Table 1).

BF were studied from 21 samples collected in ZB section. The most of the samples contain diverse foraminiferal assemblages of good preservation. More than 30 genera were identified. The foraminiferal assemblage of the interval from the base of studied succession to 9.0 m (samples 23–18) is characterized by high total abundance (700–2000 specimens) and taxonomical diversity (19–23 genera) (Fig. 8). Infaunal taxa (both shallow and deep

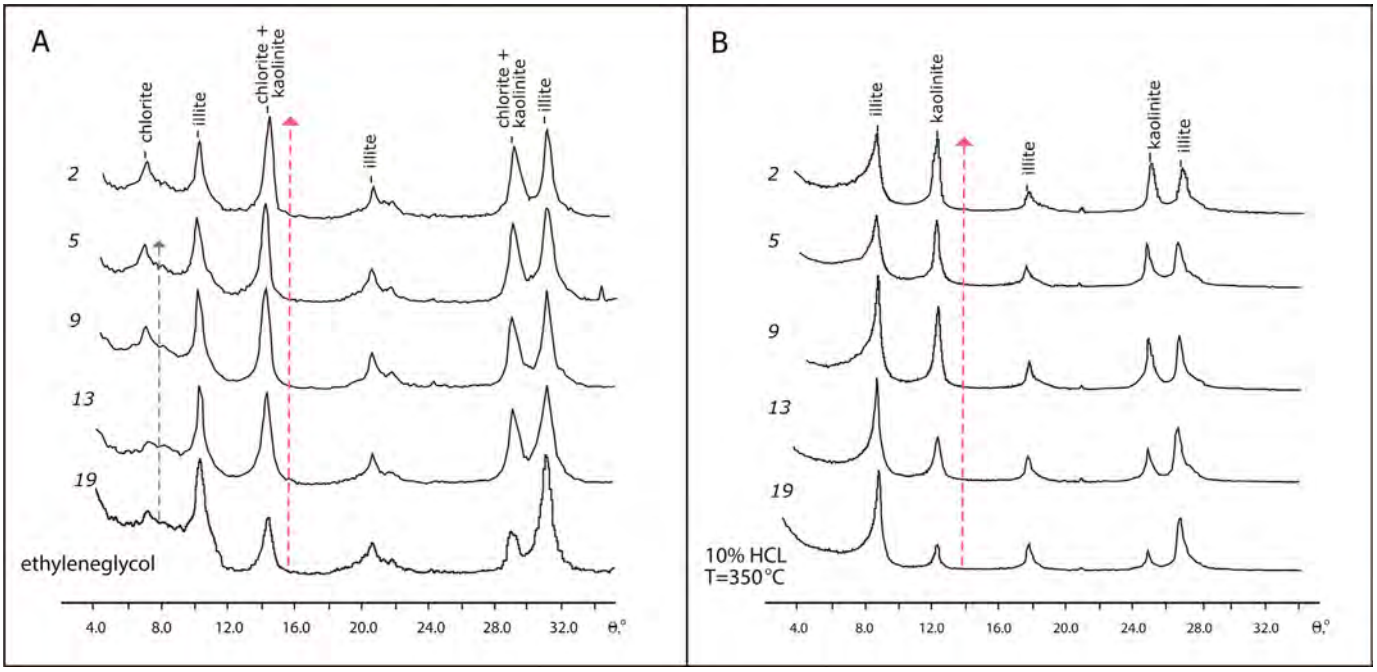

Fig. 7. XRD patterns of clay fraction (<0.002 mm) of the upper Barremian–Aptian mudrocks: A – ethyleneglycol-saturated, B – treated with 10% HCl and then heated to 350 °C for elimination of chlorite and chlorite–kaolinite mixed layered minerals. The arrows show an increase in the intensity of the XRD-peaks of kaolinite (red dotted line) and chlorite (green dotted line).

Table 1
Benthic foraminiferal morphogroups, their habitat and lifestyle (Nagy, 1992; Tyszka, 1994; Reolid et al., 2008, 2010; Nikitenko et al., 2013).

	MG		Test form	Life style	Feeding strategy	Genera
Agglutinated	A		tubular and unilocular	Epifaunal	suspensivorous	*Hyperammina*
	B		globular, pseudospheric unilocular	Epifaunal	passive detritivore s	*Saccammina*
	C	C1	elongated uniserial	shallow to deep infaunal	detritivores bacterial scavengers	*Reophax*
		C2	elongated uniserial, initial planospiral or streptospiral coiling	shallow infaunal	detritivores bacterial scavengers	*Ammobaculites*
		C3	elongated biserial, triserial and high trochospiral	shallow to deep infaunal	Detritivores bacterial scavengers	*Gaudryina* *Dorothia* *Verneuilinoides*
	D	D1	plano-convex, low trochospiral	epifaunal	active herbivores, detritivores, omnivores	*Trochammina*
		D2	rounded planispiral	epifaunal to shallow infaunal	active herbivores, detritivores, bacterivores	*Haplophragmoides* *Recurvoides*
	E		Flattened, discoidal, spiral or irregular coiled (bilocular)	epifaunal (phytal)	active herbivores, detritivores	*Ammodiscus* *Glomospira* *Glomospirella*
Calcareous	G1		low trochospiral, lenticular	epifaunal	primary weed fauna, grazing herbivores	*Gavelinella*
	H		discoidal flattened (planispiral)	epifaunal	primary weed fauna, grazing herbivores/phytodetritivores	*Spirillina*
	J	J1	elongated uniserial	shallow infaunal	active deposit feeders, herbivores, bacterial scavengers	*Dentalina* *Nodosaria* *Pseudonodosaria* *Lingulonodosaria* *Ichthyolaria* *Citharina* *Citharinella* *Marginulina* *Tristix* *Ramulina*
		J2	elongated flattened	shallow infaunal	active deposit feeders, grazing omnivores	*Astacolus* *Planularia* *Saracenaria*
		J3	spiral, sigmoidal	shallow to deep infaunal	active deposit feeders, grazing omnivores	*Globulina*
	K		biconvex (lenticular) planispiral	epifaunal to deep infaunal	active deposit feeders, grazing omnivores	*Lenticulina*

sediment dwellers) dominate in this interval (59–83%). The relative abundance of infaunal morphotypes can be used as an index of the bottom-water oxygenation and/or relative amount of OM input. The infauna dwelling the shallow depth (35–45%) is represented by morphogroups (MGs): J1, J2, C2, D2 (Fig. 9). The assemblages are composed mainly of calcareous BF as *Dentalina, Marginulina,*

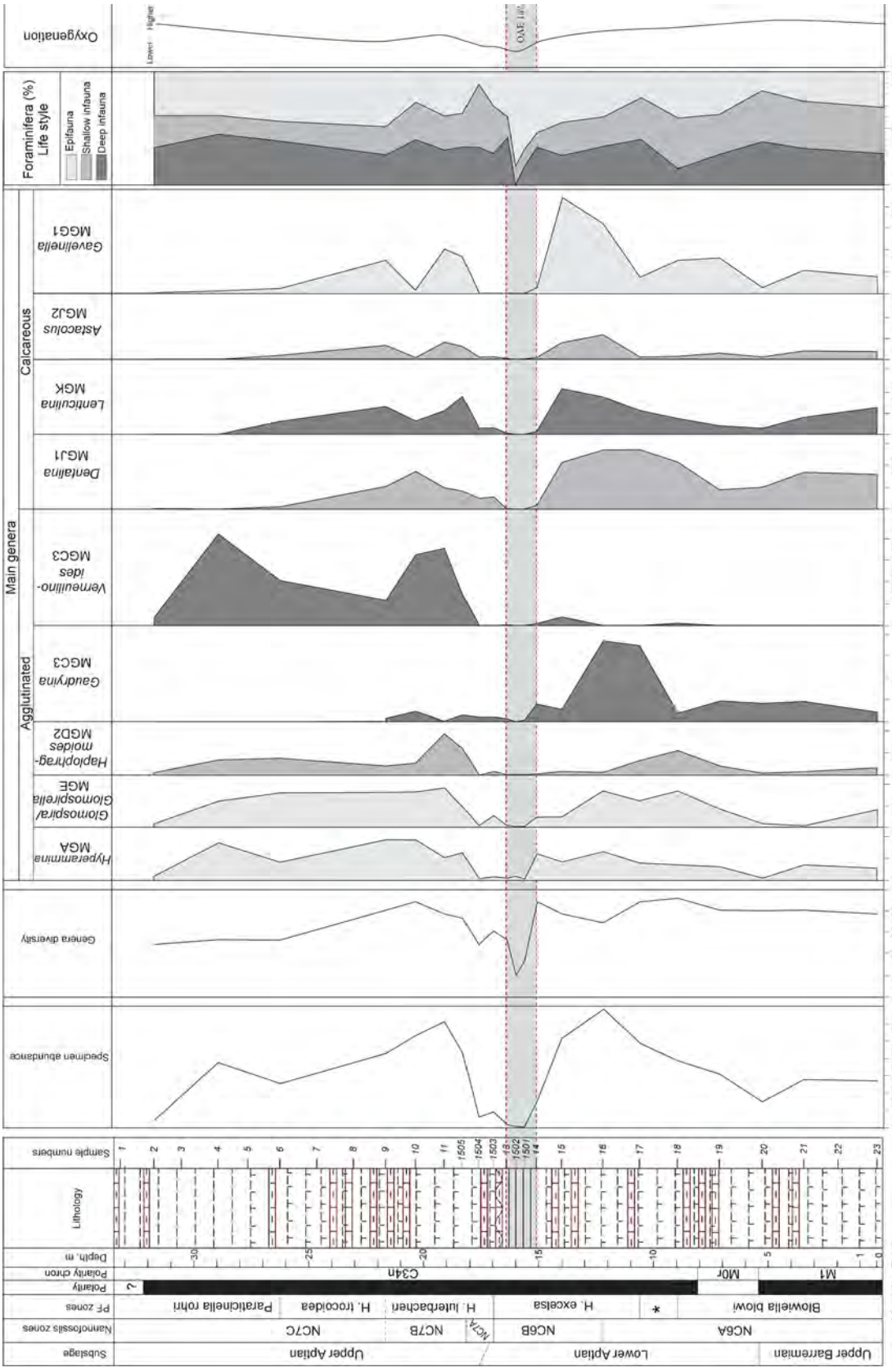

Fig. 8. Specimen quantity, generic diversity, percentage of BF epifauna, shallow and deep infauna and estimated oxygenation.

Pseudonodosaria, Nodosaria, Astacolus, Planularia, Saracenaria and agglutinated *Ammobaculites*, *Haplophragmoides.* The calcareous taxa *Citharina, Citharinella, Ramulina, Ichthyolaria, Lingulonodosaria, Tristix* are rare. The deep infauna (14–38%) is represented by agglutinated morphogroups as *Gaudryina, Dorothia, Verneuilinoides* (MGC3), *Reophax* (MGC1) and calcareous *Globulina* (MGJ3) and *Lenticulina* (MGK). The last taxon is opportunist, which seems to have tolerated a wide range of microhabitats from epifaunal to deep infaunal (Tyszka, 1994). The epifauna (17–41%) morphogroup is dominated by calcareous *Gavelinella* (MGG1) and includes agglutinated *Hyperammina* (MGA), *Ammodiscus, Glomospira, Glomospirella* (MGE), *Saccammina* (MGB) and rare *Trochammina* (MGD1). This BF assemblage characterizes relatively deep basin (middle to outer shelf?) with stable hydrodynamic conditions.

The rapid increase in total abundance (3500 specimens) and decline of taxonomical diversity (from 22 to 15 genera) are observed in the BF assemblage of the interval from ca. 10.8 to 14.0 m (samples 17–15) (Fig. 8). The infauna (54–76%), both inhabited shallow and deep depth in the sediment, dominates the BF assemblage. At the level of ca. 14 m (sample 15), the part played by epifauna increases up to 46%, mainly due to a sharp increase in the relative abundance of *Gavelinella* (Fig. 8), which is capable to occupy new ecologic niches in response to increasing food supply with decreasing oxygen level (Friedrich et al., 2006).

The level ca.15.2 m (sample 14) is characterized by rapid decrease in total foraminifer abundance (up to 780) and recovery of taxonomical diversity (22 genera) in the BF assemblage. The infauna/epifauna ratio significantly decreases and epifauna reaches 52% in the total BF assemblage (Fig. 8). The BF assemblage of the interval from ca. 15.6 to 16.0 m (samples 1501–1502) is characterized by dramatically reduced total abundance and taxonomical diversity (to 5–8 genera). At the same time, the calcareous taxa become dramatically declined and disappear in the sample 1502 (Fig. 8). The epifauna, represented mainly by primitive species of *Hyperammina* (MGA), dominates (69–84%) the assemblage. *Ammodiscus, Glomospira, Glomospirella* (MGE), *Trochammina* (MGD1) and *Saccammina* (MGB) are rare. The infauna (16–31%) is represented by scarce specimens of MGs J1, J2, C2, D2, C3. The deep infauna is not found at the level of sample 1502. Thus, the oxygenation of bottom water progressively decreases from the level ca. 10.8 m (sample 17), which culminated at the level ca. 15.6–16.0 m (samples 1501–1502). This dramatic turnover in the BF assemblages is most likely caused by oxygen deficiency at the seafloor, possibly, corresponding to OAE1a.

The gradual recovery of the total abundance (above 400) and taxonomical diversity (12–15 genera) of BF assemblage is observed in the interval from ca. 16.5 to 17.5 m (samples 13, 1503, 1504). The infaunal taxa (60–89%) dominate the assemblage (Fig. 8). The rapid increase in the total abundance (2000–3000 specimens) and taxonomical diversity (18–22 genera) in foraminiferal assemblages and sharp increase of deep burial *Verneuilinoides* occurs in the interval from ca. 18.5 to 21.8 m (samples 1505–9) that indicates the enhanced oxygenation and, possibly, eutrophy. Both epifauna (MGs: A, E, D1, B, G1) and shallow (MGs: J1, J2, F, C2, D2) and deep (MGs: C1, C3, K, J3) infauna restore their taxonomic diversity. It is noteworthy the appearance of the representatives of *Recurvoides* (MGD2) and the domination of *Verneuilinoides* over *Gaudryina* in MGC3 (Fig. 8).

The BF assemblage of the interval from ca. 26.2 to 31.8 m (samples 6, 4, 2) is characterized by decrease in total abundance (1900–1200 specimens), taxonomical diversity (12–13 genera) and relative abundance of calcareous forms. Agglutinated foraminifera dominate the BF assemblage, but rare calcareous *Gavelinella* (MGG1), *Dentalina, Citharinella* (MGJ1), *Astacolus* (MGJ2), *Lenticulina* (MGK) appear. The tests of some shells, for example, *Ammodiscus*, becomes coarser, which may indicate the intense hydrodynamics. At the level of sample 2, the BF abundance decreases significantly (to 200 specimens), which indicates unfavorable conditions for benthos.

3.2.2. Interpretation

The results obtained from BF study at ZB section enabled the recognition of the palaeoenvironmental variations during the uppermost Barremian to Aptian. In the latest Barremian to early Aptian, the BF assemblage indicates relatively deep shelf basin with stable conditions and generally transgressive trend, probably punctuated by short regressive episodes. The changes in the structure and composition of BF assemblages show the response to variations in the oxygenation at the seafloor. The significant turnover in the BF assemblage in the interval of OAE1a suggests hypoxic to anoxic conditions. In the early late Aptian, BF community becomes recovered indicating the short-term restoration of the normal bottom conditions. The followed regression leads to significant reduction in the total abundance of BF as a response to subsequent deterioration of bottom conditions.

3.3. Ostracods

3.3.1. Results

Ecological reconstructions based on ostracods were made using three parameters: specimen numbers, species diversity and eurybathic and relatively deep-water (RDW) ostracods ratio (Fig. 9).

The section begins (samples 23–22) with gradual decrease of both specimens number and species diversity accompanied with the increase of RDW ostracods, ended in sample 21 significant specimen and species number drop along with continued rise of RDW ostracods. Total rise of the latter equaled 42% from 12% to 53%. This short-term decline changed to rise of both specimen number and species diversity by the level of sample 20. Specimen abundance increased from 55 to 189, species diversity rose from 21 to 36 species. At the same level, the percentage of RDW dropped slightly down to 40%. Further up the section (samples 20–16) the specimen quantity increases gradually up to 210 specimens with unsignificant fluctuations. During the same interval species diversity declines smoothly down to 27 species. Then up to sample 15 both parameters decrease dramatically and ostracods disappear by the level of sample 14. As for RDW ostracods percentage, two cycles of increasing followed by decrease can be traced: first took place in samples 20–17, second in samples 17–14. In the first cycle the percentage rises from sample 20 to 18 from 40% to 49% and drops in sample 17 to 31%. In the second cycle the percentage goes up, in the interval of samples 17–16 it rises by 9%, then decreases slightly by the level of sample 15, and by sample 14 ostracods peter.

The interval of samples 14, 1501 and 1502 is characterized by total lack of ostracods. They reappear in tiny amount in the sample 13, where three ostracods of two species were found and one of them is *Procytherura* sp. 7 assigned to RDW ostracods. Rapid increase of both specimen and species amount is observed from the sample 13 to 1504, where absolute values reached 115 specimens of 24 species. Afterwards both parameters declined sharply to 51 and 8 correspondently. The percentage of RDW ostracods dropped to 8% in sample 1503, then restored to 30% in sample 1504 and increased slightly in 1505. In the interval of samples 1505-10 both specimen abundance and species diversity grew rapidly and reached numbers of 205 specimen belonging to 21 species. By sample 9 specimen quantity continued moderate growth up to 210 specimens, but species diversity started smooth decrease. Starting with sample 9 both parameters decline rapidly and ostracods totally disappear by sample 3. As for RDW ostracods percentage, it continued slow growth by sample 11 and reached 35%, but then demonstrated dramatic decrease, in the

interval of samples 9–7 RDW ostracods percentage did not exceed 4%. The disappear in sample 6 and do not restore by the end of the section.

3.3.1.1. Interpretation. Ostracods are very sensitive organisms to the different environmental factors, such as salinity, temperature, oxygenation, hydrology, substrate type, distance from the shoreline, depth which are usually taken into consideration in paleoecological reconstruction of ancient marine basins. Using the relative depth reconstruction method (Karpuk, 2021), the ratio of eurybathic and relatively deep-water species (Table 2) was calculated and species diversity and specimen quantity was also taken into account (Fig. 9). The increase in abundance of relatively deep-water species was considered as indication of deepening and, vice versa, their low abundance suggests shallower depth. The high total abundance and species diversity are the indicators of the stable environment and the decrease of these parameters is regarded as environment changes, whether depth, salinity or any other (Tesakova, 2014).

The presence of *Eucytherura*, *Procytherura*, *Macrocypris*, *Pontocyprella*, *Asciocythere* in the uppermost Barremian and the beginning of Aptian (NC6A, *Blowiella blowi*, *Hedbergella ruka* and beginning of *H. excelsa* zones) (0–12 m, samples 23–16, Fig. 9) in general indicates relatively deep environment, which, however, did not exceed the depth of the photic zone. In the lowermost part of the section (0–3.5 m, samples 23–21), a progressive deepening is observed. The decrease in total ostracod abundance and species diversity along with the increase of common deep-water ostracods suggests environmental stress caused by the increasing depth of the basin. Up the section, at the level of the sample 20, the increase of species diversity and total abundance and decrease of relatively deep-water genera likely implies the short-term restoration of relatively shallower depth. The new phase of the deepening is indicated by the relatively deep-water ostracod association observed in the end of *B. blowi* zone. The high ostracod abundance and ratio of relatively deep/eurybathic genera at the level of sample 18 likely suggest the adaptation of ostracod community to the deeper environment, which persisted during the whole interval of samples 19–15. The slight shallowing at the level of sample 17 is accompanied by decrease in the species and specimen abundance. In the sample 15, the species abundance drops from 27 to 19 and the specimen quantity from 210 to 86. Ostracods totally disappear in the samples 14–1502, possibly, due to the low oxygen level at the basin floor during OAE1a. A very poor ostracod assemblage, including only few specimens, reappears at the level of the sample 13. The gradual recovery of the RDW association in the beginning of the late Aptian suggests rather deep environment. At the level of the sample 11, the abundance of eurybathic species (*Robsoniella minima, R. longa*) increases and abundant new eurybathic ostracods (*Dorsocythere stafeevi*, *Saxocythere omnivaga*, *Protocythere whatleyi*) appear indicating the shallowing of the basin. The presence of ostracods with thick shells suggests the dwelling in the bottom exposed to the storm waves, i.e. in the relatively shallow depth. The short-term occurrence of favorable for ostracod conditions (samples 10–9) enabled the high species diversity (21 species) and specimen quantity (up to 210). However, the continued regression destabilized the environment. Possibly, the enhanced freshwater input resulted in the reorganization of the ostracod assemblage: the abundance and species diversity drop dramatically until ostracods became eliminated from the sample 3.

Table 2
Preferable depth of habitat and classification of ostracod genera according to this parameter. The depth estimation follows Donze (1975), Benson (1984), Hart and Crittenden (1985), Andreau (1992), Schornikov (2005), Tesakova (2014), Savelieva (2014) and personal observations of authors (M.K.).

Genus	Depth, m	Group
Cytherella Jones, 1849	Eurybathic	Shelf and eurybathic
Cytherelloidea Alexander, 1929	Relatively deep-water	Relatively deep-water
Sigillium Kuznetsova, 1960	Eurybathic	Shelf and eurybathic
Robsoniella Kuznetsova, 1956	Eurybathic	Shelf and eurybathic
Bairdia M'Coy, 1844	Eurybathic	Shelf and eurybathic
Bythocypris Brady, 1880	Eurybathic	Shelf and eurybathic
Pontocyprella Mandelstam, 1955	Eurybathic	Shelf and eurybathic
Pontocypris Sars, 1865	Eurybathic	Shelf and eurybathic
Paracypris Sars, 1865	Eurybathic	Shelf and eurybathic
Monoceratina Roth, 1928	Eurybathic	Shelf and eurybathic
Eucytherura Müller, 1894	Relatively deep-water	Relatively deep-water
Procytherura Whatley, 1970	Lower sublittoral	Relatively deep-water
Paranotacythere Bassiouni, 1974	Relatively deep-water	Relatively deep-water
Cytheropteron Sars, 1865	40–400 m, but their quantity increases with deepening under 200 m	Shelf and eurybathic
Pedicythere Eagar, 1965	Deep-water	Relatively deep-water
Loxoella Kuznetsova, 1956	Eurybathic	Shelf and eurybathic
Neocythere Mertens, 1956	up to 100	Shelf and eurybathic
Vocontiana Donze, 1968	Eurybathic	Shelf and eurybathic
Protocythere Triebel, 1938	Subittoral	Shelf and eurybathic
Hecticythere Gruendel, 1978	Subittoral	Shelf and eurybathic
Neocytherettina Lyubimova, 1965	Relatively deep-water	Relatively deep-water
Cythereis Jones, 1849	Lower sublittoral	Shelf and eurybathic
Tethysia Donze, 1975	Relatively deep-water	Relatively deep-water
Exophthalmocythere Triebel, 1938	Relatively deep-water	Relatively deep-water
Parexophtalmocythere Oertli, 1959	Relatively deep-water	Relatively deep-water
Clithrocytheridea Stephenson, 1936	Eurybathic	Shelf and eurybathic
Loxoconcha Sars, 1866	Shallow-water	Shallow-water
Macrocypris Brady, 1867	Lower sublittoral	Relatively deep-water
Bairdoppilata Coryell, Sample et Jennings, 1935	Eurybathic	Shelf and eurybathic
Schuleridea Swartz et Swain, 1946	Shallow-water	Shallow-water
Acrocythere Neale, 1960	Subittoral	Shelf and eurybathic
Rehacythereis Gruendel, 1973	Subittoral	Shelf and eurybathic
Dolocytheridea Triebel, 1938	Eurybathic	Shelf and eurybathic
Dolocythere Mertens, 1956	Subittoral	Shelf and eurybathic

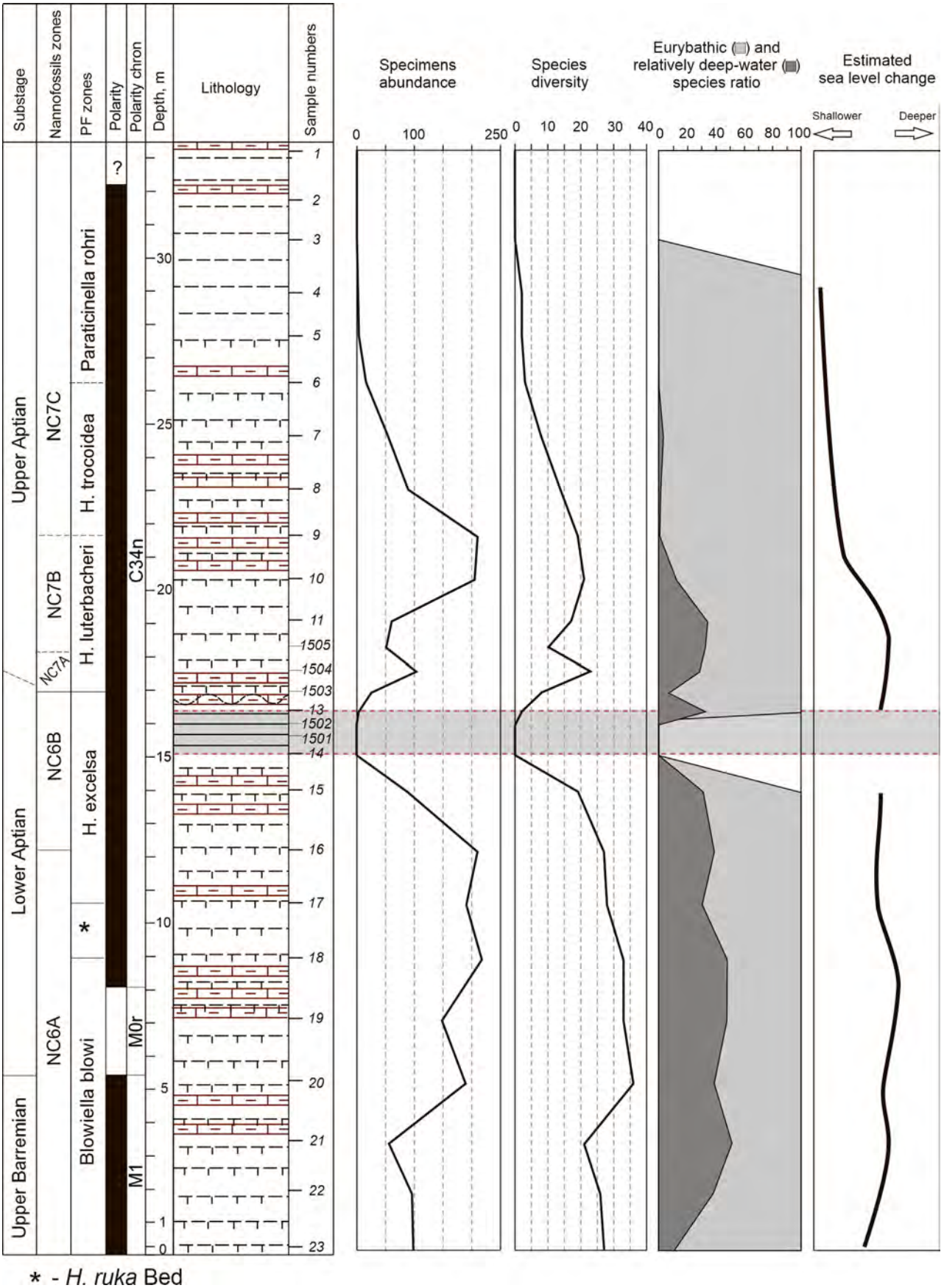

Fig. 9. Ostracod specimen abundance, species diversity, the ratio of eurybathic and relatively deep-water species and estimated sea-level trends in the ZB section.

3.4. Calcareous nannofossils

3.4.1. Results

Nannofossils were studied from all samples collected in ZB section. The most of samples contain diverse nannofossil assemblages of moderate to good preservation, but some samples are devoid of nannofossils or contain very scarce assemblage. An analysis of nannofossil stratigraphic distribution in this section defined the stratigraphic range of the studied succession as the interval of NC6A–NC7C subzones (upper Barremian to upper Aptian, Karpuk et al., 2018). The nannofossil assemblage of the interval of NC6A to lower NC6B subzones (Fig. 10) is characterized by high abundance and taxonomical diversity, which drop significantly in samples 15 and 14. The ca. 1 m thick interval (samples 1501–1502) is lack in nannofossils, which reappear in sample 13 and partially restore their numbers in the interval of samples 1503 to 8. Above this interval, nannofossil assemblage is poor to scarce.

The ratio in nannofossil paleoenvironmental indicators show the large variations through the section (Fig. 10). The lower part of the studied succession is widely dominated by *Watznaueria* and *Nannoconus*, forming together up to 80% of nannofossil assemblage. The upper part of the section (samples 1505–5) is lack in nannoconids, while *Watznaueria* are abundant. The warm-water *Rhagodiscus* spp. dominate the non-*Watznaueria*/*Nannoconus* fraction throughout the whole succession that indicates relatively warm surface water during the whole studied interval. Among commonly used nannofossil paleoecological indices, *Biscutum constans* is very scarce in ZB section, but appears in few specimens just prior and above the nannofossil-free interval within NC6B subzone (samples 16–17 and 1504–8). *Discorhabdus rotatorius* is absent from the whole studied succession.

The nannofossil assemblage of the interval of NC6A subzone is characterized by high abundance and taxonomical diversity. This assemblage is dominated by two inversely correlated taxa *Watznaueria* and *Nannoconus*, which show significant variations in their relative abundance. The main part in the non-*Watznaueria* and *Nannoconus* fraction is played by *Rhagodiscus* (40–73%), while the relative abundance of each other taxon from this fraction does not exceed 12–20%. *Assipetra* spp., pentaliths (mainly *Micrantolithus*), small *Zeugrhabdotus* (*Z. erectus, Z. diplogrammus, Z. howei*) and *Lithraphidites carniolensis* are present in low relative abundance (not more than 10%), showing the inversed correlation with the fluctuations in the relative abundance of nannoconids.

The beginning of NC6B is marked with major reduce followed by total disappearance of nannoconids (samples 16–15). The interval from ca. 15.0 to 17.5 m (samples 14–13) demonstrates dramatically reduced total nannofossil abundance up to the total nannofossil elimination from the samples 1501–1502 (ca.15.6–16.0 m). The base and the top of this interval are featured by typical for OAE1a variations in the composition of nannofossil assemblage – increase of *Assipetra* and *Rucinolithus* abundance, including occurrence of large specimens of *A. infracretacea larsonii* and *R. terebrodentarius youngii*, and the absence of pentaliths. The inverse correlation of *Nannoconus* spp. and *Assipetra*/*Rucinolithus* spp. is observed in many Tethyan sections (Erba, 1994; Aguado et al., 1999; Bellanca et al., 2002; Barragan and Melinte, 2006; Tremolada et al., 2006).

The gradual recovery of nannofossil abundance above the interval of OAE1a was accompanied by the restoration of high relative abundance of warm-water *Rhagodiscus* and *Assipetra*/*Rucinolithus*. The return of nannoconids, although in minor abundance, is found in the interval of samples 1503–11 (NC7A–B subzones, lower part of the upper Aptian), where they show again inversed correlation with *Assipetra*. The re-entry of *Nannoconus* above the OAE1a detected in the Tethys, Boreal Realm and Pacific Ocean (e.g. Erba 1994; Erba and Tremolada, 2004; Erba et al., 2010; Bottini and Mutterlose, 2012).

Further up the section (samples 7–5), the taxonomically poor assemblage widely dominated by eyritopic *Watznaueria* is found. Only few nannofossil specimens are found in the uppermost part of the studied section (samples 4–2).

3.4.2. Ecological affinity of nannofossil taxa

Some nannofossil taxa are widely used as paleoenvironmental indices. *Watznaueria* spp. are widely present in the Cretaceous deposits, but their paleoecological affinity remains questionable. Some researchers consider this taxon tending to high-fertility conditions (Luciani et al., 2001; Suchéras-Marx et al., 2015) or indicating low surface water productivity (Mutterlose et al., 2005). On the other hand, *Watznaueria* show inversed correlations with the euthrophic/mesotrophic taxa that suggests their oligotrophic affinity (Roth and Krumbach, 1986; Erba, 1992; Fisher and Hay, 1999; Herrle and Mutterlose, 2003). These controversial interpretations likely suggest *Watznaueria* is rather eurytopic taxon, the most resistant to paleoecological perturbations (Lees et al., 2005; Barragan and Melinte, 2006; Aguado et al., 2014). Besides, *Watznaueria* spp. is the most resistant to diagenetic alternations (dissolution and overgrouth) taxon among Mesozoic nannofossils (Roth and Bowdler, 1981; Roth and Krumbach, 1986; Erba, 1992), which dominates the nannofossil assemblages in poorly preserved material. The nannofossils observed in ZB section do not display visible diagenetic alternation and dissolution-susceptible taxa (small *Zeugrhabdotus*, *Staurolithites*) are present. Thus, the variations in *Watznaueria* specimen numbers can be considered here as the changes in the primary productivity under unstable paleoecological conditions, when this taxon can replace the more selective species.

Nannoconids are belived to be warm-water oligotrophic species, dwelling the lower photic zone (Erba, 1992, 1994; Melinte and Mutterlose, 2001; Herrle et al., 2003; Tremolada et al., 2006). *Ragodiscus* is considered as warm water indicator, while *Eprolithus* tends to cool water conditions (Roth and Krumbach, 1986; Erba, 1992; Bralower, 1988; Herrle and Mutterlose, 2003; Mutterlose et al., 2005; Aguado et al., 2014, a.o.). Small *Zeugrhabdotus* spp., *Biscutum constans* and *Discorhabdus rotatorius* are considered as indicators of increased fertility (Roth and Bowdler, 1981; Roth and Krumbach, 1986; Erba, 1992; Herrle and Mutterlose, 2003, a.o.). *B. constans* prefers higher fertilization than *Zeugrabdotus* at that (Fischer and Hay, 1999). *Lithraphidites carniolensis* and *Micrantolithus* spp. have no clear paleoecological affinities: the first species is suggested to be indicative of moderate fertility (Erba, 1992; Luciani et al., 2001; Peybernes et al., 2013) and the last one is considered as tending to warm water (Melinte and Mutterlose, 2001) and oligotrophic conditions, showing direct positive correlation with variations in *Nannoconus* relative abundance (Erba, 1994; Erba and Tremolada, 2004; Quijano et al., 2012; Aguado et al., 2014). *Assipetra* and *Rucinolithus* spp. tend to open-ocean settings (Lees et al., 2005; Aguado et al., 2014) and, possibly, to enhanced fertilization (Patruno et al., 2015), displaying inversed correlation with nannoconids and increased relative abundance around OAE1a (Erba, 1994; Tremolada et al., 2006; Quijano et al., 2012; Aguado et al., 2014).

The variations in the productivity of surface water can be estimated through the changes in nutrient index (NI) formulated as (Herrle et al., 2003, Bottini and Erba, 2018):

$$NI = (Bc + Ze + Dr) : (Ze + Dr + Wb) \times 100$$

where Bc labels *Biscutum constans*, Ze – *Zeugrhabdotus erectus*, Dr – *Discorhabdus rotatorius*, Wb – *Watznaueria barnesae*. In our counts, we included not only *Z. erectus*, but all small *Zeugrhabdotus* (<5

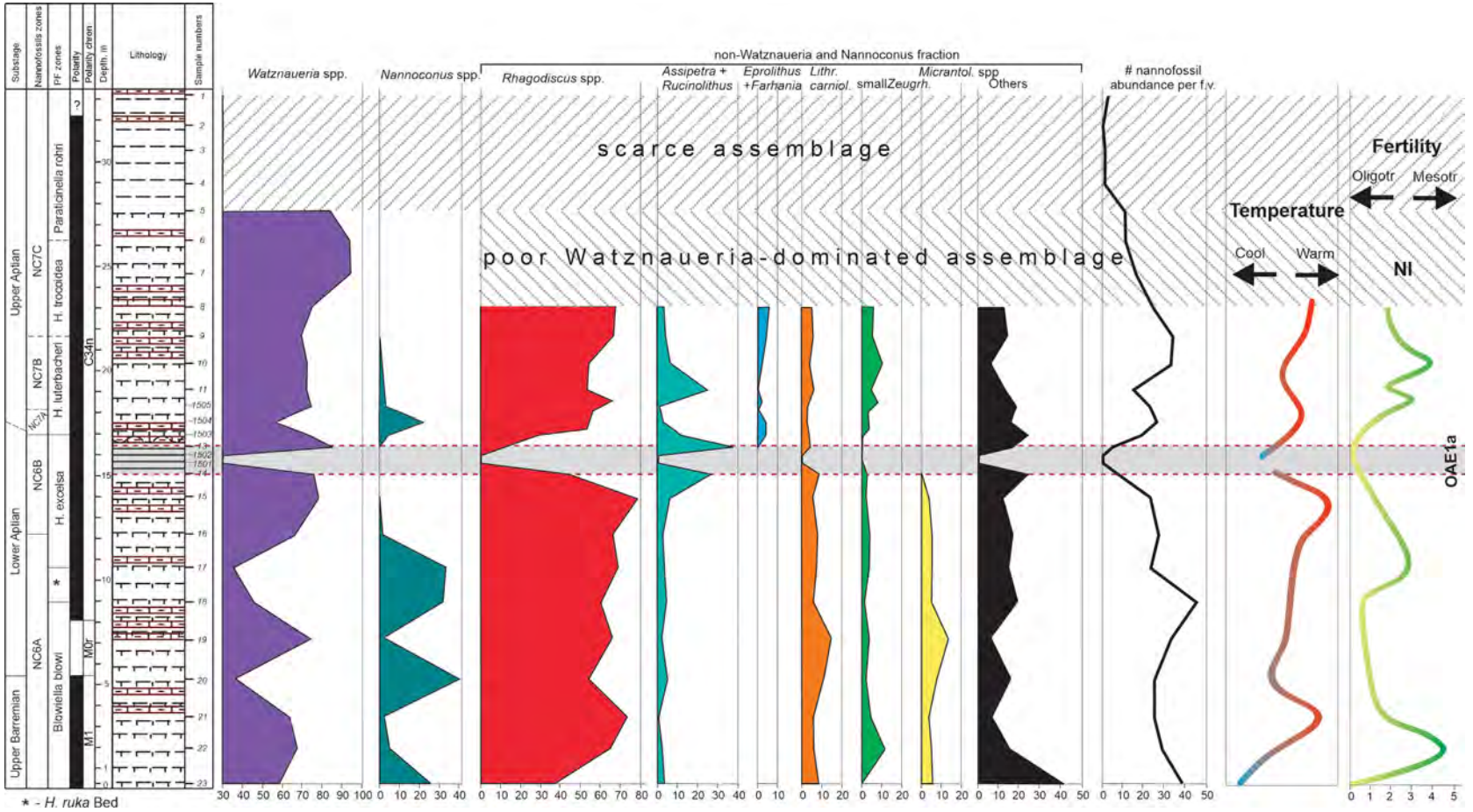

Fig. 10. Relative (%) total abundance of nannofossil ecological indicators, total nannofossil abundance per field of view (FOV) counted from 50 FOV, temperature variations estimated by the changes in the relative abundance of *Rhagodiscus* spp. and Nutrient Index (NI), calculated according to Herrle et al. (2003).

μm), which are believed to be eutrophic species (Lees et al., 2005; Aguado et al., 2018; Kanungo et al., 2018; Jaillard et al., 2019).

3.4.3. Interpretation

The results obtained from nannofossil study of ZB section revealed a series of paleoecological variations during the uppermost Barremian–Aptian. In the latest Barremian to early early Aptian (NC6A subzone), major variations of *Watznaueria* and *Nannoconus* in the lower part of the section (NC6A) is, possibly, related to the changes in the depth and nutrification of the basin: the higher percentage of nannoconids more likely corresponds to more oligotrophic conditions and/or deeper neritic settings. The composition of non-*Watznaueria* assemblage likely suggests warm oligotrophic to mesotrophic conditions in the early Aptian. The significantly decreased nannoconid abundance at the levels of samples 22–21 and 19 (3.0—4.5 and 7.3 m, respectively) more likely corresponds to the episodes of the short-term shallowing of the basin, which caused the restriction of the favorable for *Nannoconus* spp. habitat, specifically, deep nutricline. The heavily calcified *Nannoconus* spp. were important producers of $CaCO_3$ in the marine basins, that is why the decrease in their abundance resulted in the lower values of calcium carbonate at these levels (see Fig. 3). The level of most abundant nannoconid specimens corresponding to the highest nannofossil abundance (ca. 9.0 m, sample 18), likely pointes to greater distance from shoreline, deeper and, possibly, more oligotrophic environment indicated by low NI.

The dramatic elimination of nannoconids at the level ca.12 m (sample 16) corresponds to the widely known “nannoconid crisis”, which precedes the onset of OAE1a in many areas (e.g., Erba, 1994; Erba et al., 1995; Aguado et al., 1999, 2014; Channell et al., 2000; Quijano et al., 2012; McAnena et al., 2013; Bottini et al., 2015, Patruno et al., 2015; a.o.). This event is interpreted as biocalcification crisis accompanied by surface-water nutrification, triggering bloom of surface water nannoplankton and depletion of deeper-dwelling nannoconids (Erba, 1994; Méhay et al., 2009). *Micrantolithus* spp. show the same trend to decline toward the middle part of NC6B subzone (sample 14, ca. 15.1 m). The highest relative abundance of *Rhagodiscus* in this interval evidences the warmest temperature followed the onset of “nannoconid crisis”.

The decrease in abundance of the warm-water *Rhagodiscus* in the samples 14 and 13 is accompanied by the occurrence of rare cool-water *Repagulum parvidentatum*, which is absent from all other parts of the section, that suggests a relative cooling or temporal intrusion of cool waters, which could be caused by enhanced connection with Boreal realm. This is consistent with the short-term cooling during OAE1a, which was recognized in the different areas (Erba, 1994; Aguado et al., 1999; Tremolada and Erba, 2002; Herrle and Mutterlose, 2003; Kuhnt et al., 2011; Bottini et al., 2015; Bonin et al., 2016; Erba et al., 2019). The relative abundance of eutrophic small *Zeugrhabdotus* spp. at the base and the top of the interval corresponding to OAE1a is slightly lower than in embedding sediments. This indicates reduced fertilization (low NI) contrary to mesotrophic conditions of the surface water during OAE1a recently documented in the Tethyan and Boreal Realms (Luciani et al., 2001; Heimhofer et al., 2006; Bottini and Mutterlose, 2012; Aguado et al., 2014; Bottini et al., 2015). The following stratigraphic interval of the studied section (NC7A—B subzones, samples 1503–11) likely corresponds to relatively warm and deeper environment or larger distance from the shoreline. The higher relative abundance of small *Zeugrhabdotus* spp. at the later stage of this interval indicates increased fertilization (high NI), coinciding with the decline of *Nannoconus* and *Assipetra/Rucinolithus* that likely suggests sea-level fall. No *N. truittii* acme, widely documented worldwide (Erba, 1994; Herrle and Mutterlose, 2003; Bottini et al., 2015; Erba et al., 2015; Patruno et al., 2015), is found in ZB section, more likely, due to progressive shallowing of the basin in the middle late Aptian.

Further bloom of eyritopic *Watznaueria,* occupying all ecological niches available, dominating further (samples 7—5) represents the large spectrum of environmental perturbations (oligotrophication, eutrophication, fresh water input, etc.). Uppermost part of the section is characterized by mostly lack of nannofossils that signalizes the occurrence of inappropriate conditions for nannoplankton habitat and/or their reduced accumulation rate. Inferred from geochemical proxies (Fig. 3) it is more likely due to progressive shallowing of the basin and enhanced turbulence of the water.

The estimation of the fertility variations in the east Crimean basin shows mainly oligo-mesotrophic environment during late Barremian to early late Aptian. More oligotrophic conditions during the early early Aptian (NC6a zone) correspond to the high abundance of nannoconids. The enhanced oligotrophy at the OAE1a onset and recovery is less understood; evidently, it was caused by limitations in nutrients of whatever nature (reduced supply from the adjacent land, reorganization in the hydrology of the basin, etc.).

To summarize, the study of nannofossil revealed a series of paleoecological variations during the uppermost Barremian–Aptian. In the latest Barremian to early early Aptian (NC6A subzone), common nannoconids indicate hemipelagic depth with probable short episodes of the relative shallowing, culminated prior to the onset of OAE1a. During this time, the basin was featured by warm and rather oligotrophic/mesotrophic conditions, showing a trend to increased temperature by the onset of OAE1a (lower NC6B subzone). The interval of OAE1a (upper NC6B subzone) is featured by slightly decreased fertilization at the onset and termination of OAE1a, but no information can be obtained from the core of this critical event because it is lack in nannofossils. The OAE1a in the eastern Crimea basin likely occurred against the background of slight relative cooling and deepening of the basin inferred from geochemical proxies, but the driving mechanisms of dramatic nannoplankton elimination from the sediment during OAE1a are poorly understood. Both dissolution and occurrence of inhospitable environment cannot be excluded. The short-time nannofossil restoration after the crisis (NC7A–B subzones) was accompanied by a relative warming and increased nutrient input. The progressive decline of nannofossil total abundance and species diversity in the latest Aptian (NC7C subzone) was likely caused by significant shallowing of the basin and occurrence of new critical for nannofossil environment.

3.5. Planktonic foraminifera

3.5.1. Results

The taxonomical composition of planktonic foraminifera (PF) assemblage and the ratio of plaktonic and benthic taxa were investigated from all samples collected in ZB section. The PF show moderate to good preservation and wide variations in the abundance and species diversity in the uppermost Barremian to upper Aptian. Only few specimens of PF (*Hedbergella infracretacea* and *Blowiella blowi*) were found in the Barremian deposits. The progressive increase in PF abundance is observed up to the middle upper Aptian with dramatic decline at the level corresponding to OAE1a. The major drop in the foraminiferal abundance also occurs in the upper part of the upper Aptian.

The PF assemblage is represented mainly by few species of *Hedbergella*. In general, hedbergellids appeared in the beginning of the Early Cretaceous and evolved during this period, but the most rapid *Hedbergella* evolution occurred in the Aptian. In the Barremian and early Aptian, this taxon was characterized by low abundance and diversity. The bloom of PF and hedbergellids is observed

worldwide in the late Aptian (Leckie, 1989; Aguado et al., 1992; Coccioni et al., 1992, 2006). This trend is apparent in ZB section (Fig. 11).

The lower part of the section (0–7 m, samples 23–19) is represented by only two genera *Blowiella* and *Hedbergella,* showing constantly low abundance in this interval. Upsection, at the level 9 m (sample 18), poor *Blowiella* finaly disappear and eutrophic *Hedbergella* gradually increase their abundance reaching dramatic bloom at the level 14 m (sample 15). Noteworthy, almost the half of *Hedbergella* specimens are juveniles at the level 12.5 m (sample 16). Further up the section, in samples 14–13 major decrease of PF is observed, which is changed by fast and significant rise starting from sample 1503. This sample is characterized not just by major increase of PF abundance, but also by appearance of juvenile

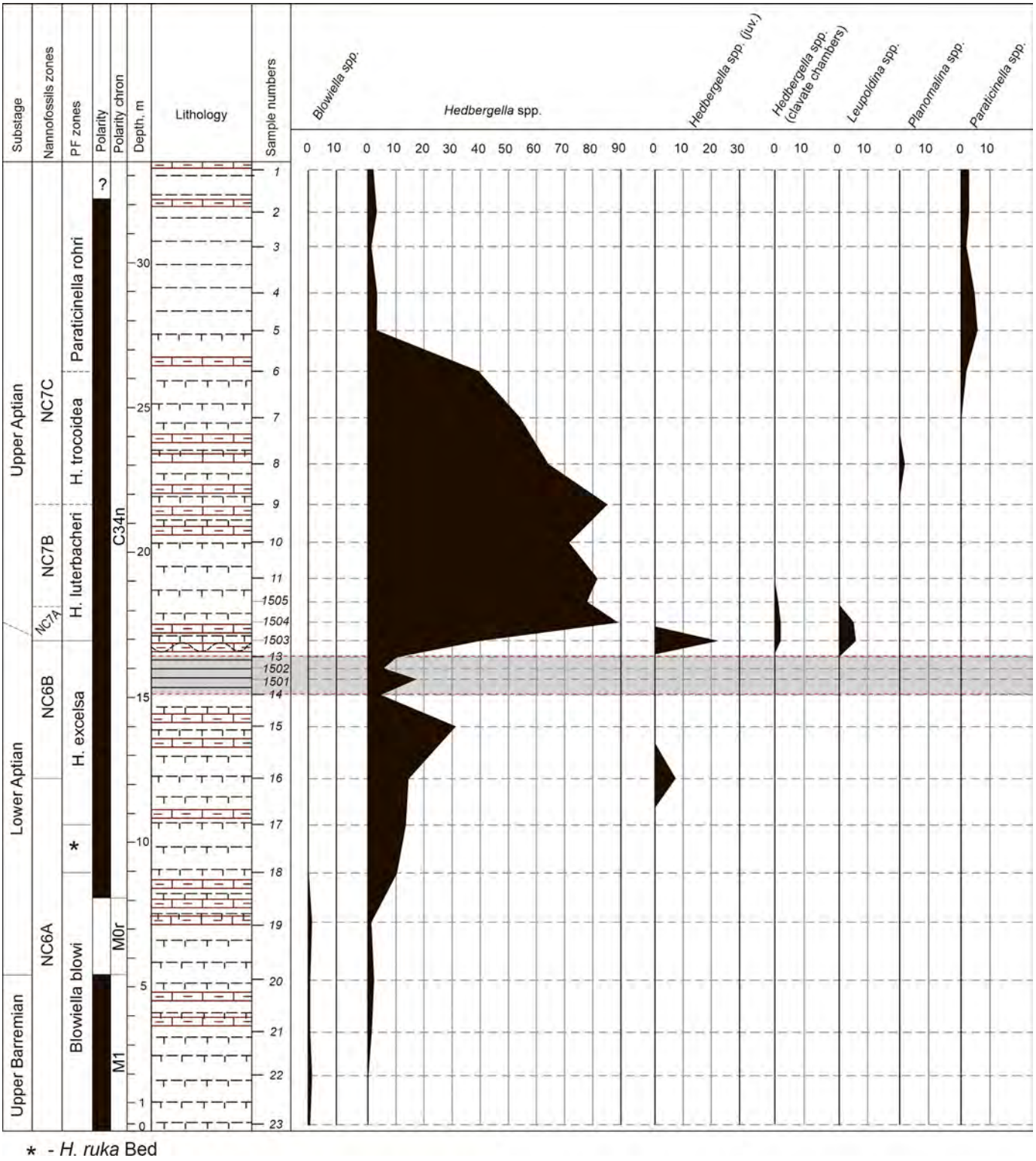

Fig. 11. Percentage of PF genera and juvenile forms of *Hedbergella* spp. in ZB section.

Hedbergella spp., *Leupoldina* spp. and hedbergellas with clavate chambers. PF with elongated chambers appear also in samples 1504 and 1505, then disappear and never restore again in the section. The amount of hedbergellas remain high with unsignificant fluctuations up to sample 9. The followed interval (samples 9–5) is characterized by certain decrease and ends with an interval of approximately stable low abundance. In sample 8 a short appearance of deeper water dwellers *Planomalina* spp. is observed. Deeper water dwellers *Paraticinella* spp. first appear in sample 6 and remain important elements of the assemblage.

3.5.2. Interpretation

Poor in abundance and genera diversity assemblage of lower part of the section is quite usual for upper Barremian–lower Aptian. After disappearance of *Blowiella* spp., and slight increase of *Hedbergella* spp., an episode of juvenile hedbergellas appearance calls attention, which could possibly mean the r-strategy adaptation or at least evidence such environmental perturbations, which prevented the PF growing-up. This assemblage corresponds to the nannoconid crisis and significant increase in percentage of benthic infauna (see above). The dramatic drop of PF abundance in the end of *H. excelsa* zone coincides with OAE1a. Yet such major decrease most likely suggests further dissolving rather than total lack of living PF and nannoplankton in the surface water at that time. The rapid increase in abundance of *Hedbergella* immediately above OAE1a is accompanied by new increase of juveniles and occurrence of rare *Leupoldina* and *Hedbergella* with clavate chambers. The chamber elongation of the early Cretaceous planktonic foraminifera has been interpreted as an adaptive response to oxygen depletion in the upper water column (Coccioni et al., 2006 and references therein). The occurrence of such specimens can signify that oxygen deficiency persisted in the water column after the termination of OAE1a main phase. The high PF abundance in the lower part of the upper Aptian (17.5–21.5 m, samples 1503–9) indicates the restoration of the normal shelf conditions. The absence of multichambered *Globigerinelloides* spp., which are assumed to be deeper water dwellers (Leckie, 1987), can be caused by the shallow paleodepth. In the beginning of *H. trocoidea* zone, few deeper water dwellers *Planomalina* occur. Rare juvenile forms of *Paraticinella*, which are believed to prefer oligotrophic conditions, appear at the level of 26.5 m (sample 6). *Hedbergella* abundance dramatically drops at the level 27.5 m and the uppermost part of the section is characterized by very poor assemblage containing almost equal quantities of *Hedbergella* and *Paraticinella*. As Aptian hedbergellids had high potency to adapt to a large spectrum of environmental variations (Luciani et al., 2001), their decline likely signalizes the significant perturbations in the climatic and/or paleoceanographic conditions.

3.6. Palynology

The palynological study of the samples from ZB section revealed two palynological assemblages (PA) (Fig. 12.). The domination of spores and pollen grains over dinocysts and high amount of the fragments of plant tissue and coal particles in both assemblages suggest nearshore accumulation of the upper Barremian–Aptian deposits. High palynomorph abundance and their co-occurrence with the particles of plant tissue and coal suggests mixed humus-leptynite-sapropelitic composition of OM in the upper Barremian to lower Aptian part of the section (samples 23–12). The humus component dominates in the upper Aptian part of succession.

The first assemblage (PA1) is recognized in the lower 7 m (samples 23–19) of the succession exposed. It is characterized by high total abundance of palynomorphs widely dominated by gemnosperms pollen (see palynomorph range charts in Karpuk et al., 2018). The taxonomic and quantitative composition of the spore and pollen spectrum indicate dry subtropical to tropical climate. The abundant *Classopollis* pollen, accompanied by diverse spores, point at the wide adjacent lowlands, possibly, indented by lagoons (Alvin, 1982; Francis, 1983; Abbink et al., 2001, 2004).

The second assemblage (PA2) is observed in the upper part of the section (10–33 m, samples 17–1). It is characterized by abundant bisaccate pollens of gymnosperms and spores of Gleicheniaceae. The common occurrence of bisaccate pollen is featured for temperate and humid climates (Keller et al., 2011). However, the exceptionally high abundance of bissacate grains (from 56 to 93% of the whole spectrum in the interval of samples 17–14) can be the result of their easier transportation, which could cause the over-enrichment of sediments by the pollen of this type during large-scale regression. This phenomenon, known under the name 'Neves effect' (e.g. Chaloner, 1958; Abbink et al., 2004; Traverse, 2007; Schrank, 2010), likely indicates the lowland drowning. It is possible, that major transgression led to lowland flooding, and the shore-line likely approached the hinterland heights, where conifers with dissacites pollen were growing.

3.6.1. Interpretation

The high abundance of palynomorphs and low percentage of dinocysts within the interval of OAE1a indicate increased terrestrial runoff, which could cause the water column stratification. The occurrence of few *Tasmanites* and amorphous OM, as well as heavy corrosion and pyritization of dinocysts likely suggests bottom stagnation affected post mortem alteration of the latter. *Classopollis* is rare in this part of the succession, but show dramatically increased abundance at the later stage of OAE1a. This likely suggests short-term restoration of pre-OAE1a terrestrial climatic conditions. At the level 18 m (sample 1504), *Classopolis* abundance drastically drops and they become extinct at the level 25 m (sample 7) that testifies dramatic climatic change from semi-arid to humid. In the middle and upper parts of the upper Aptian, common bissacate pollen of Pinaceae and Podocarpaceae associated with Gleicheniaceae testify increased humidity and warming with simultaneous expansion of open landscape on the adjacent land. The occurrence of the wide open space was more likely caused by the large-scale regression caused the emersion of the wide area, which was colonized by Gleicheniaceae as pioneer plant community.

Dinocysts are rather rare in ZB section (Karpuk et al., 2018) and their portion does not exceed 30% of the total palynomorph abundance (Fig. 12). The occurrence of *Cribroperidinium, Cleistosphaeridium, Pterodinium, Spiniferites* indicates shelf environment (Williams, 2003). The low dinocyst abundance in the interval of OAE1a (samples 14 and 13) likely suggests sea-level low-stand during this event. It is immediately followed by increase in abundance (17.5–23.0 m, samples 12–8) corresponding to the transgressive pulse. Above this interval, dinocyst association becomes very poor. The occurrence of scarce specimens of *Subtilisphaera perlucida, Protoellipsodinium spinocristatum* and common phycomata green algae in the middle part of the upper Aptian evidence shallow depth and increased fresh-water supply into the basin. In the topmost part of the succession (samples 3–1), the domination of humus component in the OM, low total palynomorph abundance and relative spore abundance and their poor preservation likely indicate very shallow depth; wide occurrence of green algae possibly evidences fresh-water impact.

3.7. Stable isotopes

The composition of carbon and oxygen isotopes was measured in the BF shells and bulk carbonate composed mainly of PF and calcareous nannofossils. The BF $\delta^{13}C$ values lie in the range from

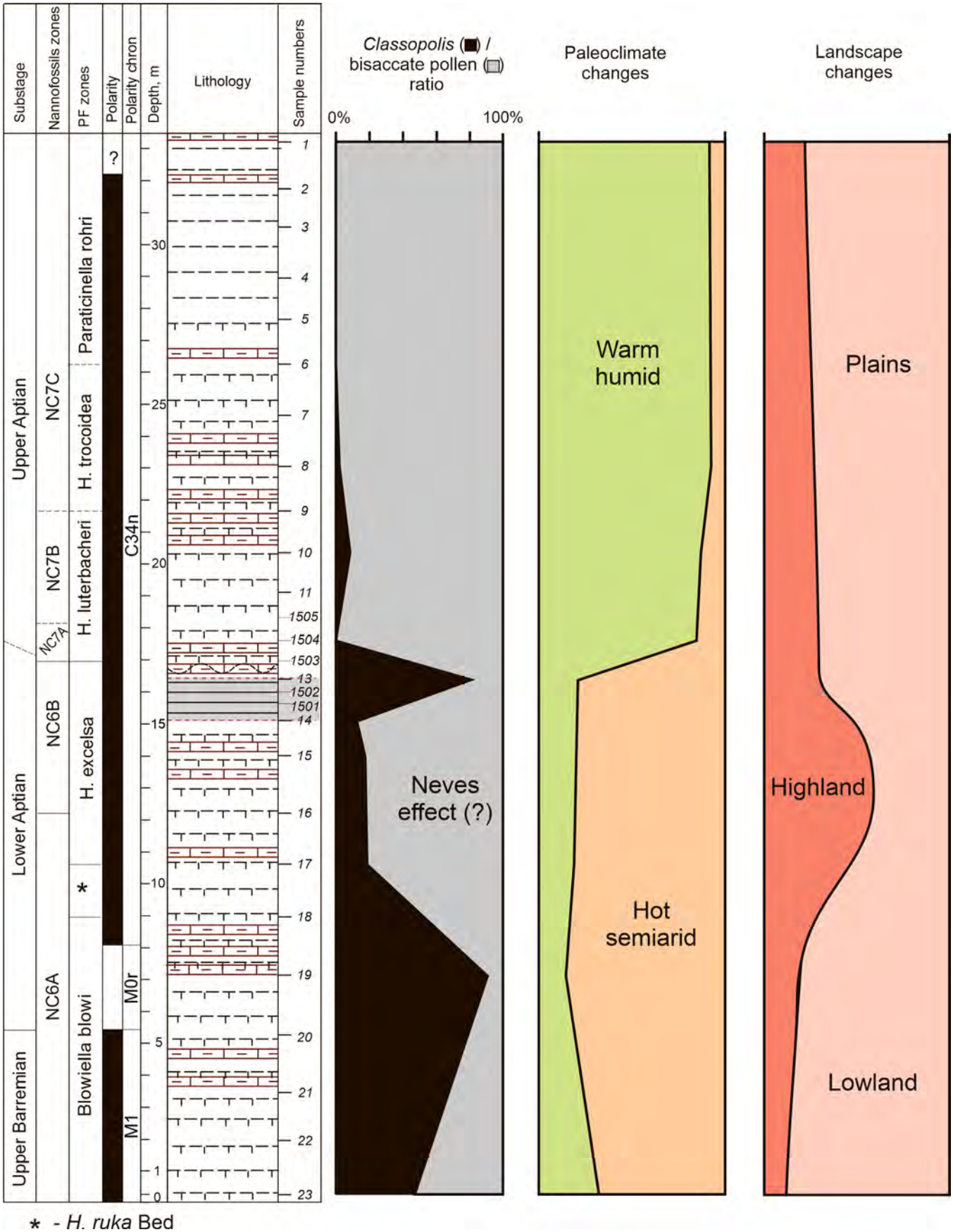

Fig. 12. *Classopolis* and bisaccate pollen ratio, paleoclimatic and landscape reconstruction.

−5.4 to 0.8 (‰ V-PDB) (Table A.3) and the bulk carbonate − from 1.1 to 4.5‰. The BF $\delta^{18}O$ varies from −4.7 to 0.6 (‰ V-PDB) and bulk carbonate − from −0.1 to 5.1‰ (Fig. 13). The upper Barremian−lower Aptian part of the section show rather stable $\delta^{13}C$ and $\delta^{18}O$ values, but they vary dramatically in the upper Aptian. The $\delta^{13}C$ values of the bulk carbonate (microplankton) are 3.2 ± 0.2‰ higher on average than $\delta^{13}C$ of BF carbonate. This difference coincides with the normal distribution of the isotope composition of dissolved inorganic carbon in the sea water column (Kroopnick, 1985; Mackensen et al., 1993; Mackensen and Schmiedl, 2019). The surface waters are more saturated in ^{13}C as a result of selective sequestration of ^{12}C during photosynthesis, and ^{12}C-rich carbon dioxide re-enter due to OM oxygenation in the bottom water. Just above low-calcareous interval at the uppermost lower Aptian, this difference increases up to 4.9−7‰, probably, due to high TOC content in the primary sediment.

The $\delta^{18}O$ values are rather stable in the lower part of section varying in the range 1.2−1.6‰. Using the relationship of Epstein et al. (1953).

$$T^{o}C = 16.5-4.3\,(\delta^{18}O_{cal} - \delta^{18}O_{water}) + 0.14\,(\delta^{18}O_{cal} - \delta^{18}O_{water})^2,$$

where $\delta^{18}O_{cal}$ is the value measured in calcite and $\delta^{18}O_{water}$ is −1.1‰ − an average $\delta^{18}O$ (‰ V-SMOW) value of oceanic water in the Cretaceous in polar ice-free world (Spicer and Herman, 2010; Herman and Spicer, 2010; Grossman and Joachimski, 2020), we obtain the temperature of surficial water 22 ± 2 °C that looks realistic for a Greenhouse World. At the same time, the temperature of the bottom water ~30 °C measured from BF seems unlikely high. This can be caused by the filling of BF tests by diagenetic calcite poor in ^{18}O due to the interaction with atmospheric water after the sediment emergence.

The absence of calcite from the OAE1a deposits caused the gap in the measurement of $\delta^{13}C$ and $\delta^{18}O$ values. The temperature of surface water after OAE1a varies wildly from 14 to 22 °C tending to decrease toward the top of the section. The estimated temperature of bottom water remains unreliably high. Only in three uppermost samples the temperature seems to be close to real (Fig. 14).

3.7.1. Interpretation

OAEs are usually featured by the positive excursions of $\delta^{13}C$ resulting from increasing burial rate of OM depleted in $\delta^{13}C$ (Des Marais, 2001). Aptian event OAE1a is characterized by dramatic variations in $\delta^{13}C$ documented in oceanic and inland Aptian successions (Menegatti et al., 1998; Lubke and Mutterlose, 2016; Naafs and Pancost, 2016; Fu et al., 2020, a. o.). In the section studied, the interval corresponding to OAE1a is low-calcareous that makes the reliable stable isotopes measurements difficult. Despite the absence of stable isotope results from the OAE1a interval at ZB section, the $\delta^{13}C$ variations around this level are in good correlation with the results obtained in other Tethyan basins (Menegatti et al., 1998; de Gea et al., 2003; Herrle et al., 2010; Hu et al., 2012) (Fig. 14). The Barremian and lower Aptian parts of the section display $\delta^{13}C$ variations of magnitude, which do not exceed 0.9‰. The interval of samples 23–19 likely corresponds to the segments C1−C2 of Menegatti et al. (1998) and the interval of negative values before OAE1a − to the segment C3. At the same time, the $\delta^{13}C$ values from the deposits above the OAE1a show significant fluctuations similar to segments C7, C8 and C9 (Table A.3).

4. Discussion

The deposits of the studied section in general were accumulated in the distant off-shore area, featured by poor sedimentary response to the sea-level variations. This caused a relatively stable supply of the well-sorted fine terrigenous material in this part of the basin despite a broad migration of the coastal line during sea-level fluctuations. Calcium carbonate content, being composed mainly of biogenic calcite, show significant variations controlled by changes in the productivity of calcareous microbiota.

The upper Barremian–lower Aptian part of the section (0−12 m) is characterized by rather stable depth not less than 80 m with minor variations, normal oxygenation of bottom water, high temperature and high productivity of both planktonic and benthic communities. High relative abundance of oligotrophic hemipelagic *Nannoconus* indicates normal marine environment. The progressive increase in abundance of deep-water ostracods and sediment granulometry denote a transgressive trend culminated in the middle lower Aptian (sample 18) (Fig. 15). The coastal areas represented lowlands covered by coniferous vegetation (mostly present by *Classopolis* genus) indicating hot arid climate. The conifer forests were widely distributed on the islands of the NE Peri-Tethys and adjacent land during the lower Cretaceous (Benenson, 1985; Vakhrameev, 1991; Duuc, 2002; Philippe et al., 2006). The relative abundance of *Classopollis* pollen dramatically reduces in the upper lower Aptian due to significantly increased abundance of gymnosperms indicative for high open spaces. This suggests the rise of the highland in the coastal area coherent with progressive shallowing of the basin caused by eustatic regression and basinward moving of the coastal line in the late early Aptian.

In the interval of OAE1a, non-calcareous clay with low TOC content accumulated. The dramatic decrease in the value of biogenic calcite in the OAE1a deposits is related with the catastrophic drop in the productivity of the calcareous microbiota. The collapse in the calcite producing microorganisms could be caused by both oversaturation of the atmosphere in CO_2 and related increase in sea-water *p*H occurred during this critical event (Erba, 1994; Weissert and Erba, 2004) or the carbonate dissolution at the sea-floor (Slater et al., 2022) mask the real carbonate production. The bottom water was not fully anoxic, but occurrence of dysoxia can be suggested from the specific BF community and domination of amorphous (more likely, algal) OM at the level of OAE1a, although the TOC content remains to be low. Generally, the OAE1a is characterized by widely increased fertilization of the oceanic basins. However, a strongly oligotrophic environment during OAE1a was registered in the Vocontian basin (Giraud et al., 2018), where TOC-rich black shales accumulated. The specific repercussion of OAE1a in the basin of the eastern Crimea could be caused by the interplay of eustatic, tectonic and climatic factors. We suggest that during the large-scale eustatic transgression, corresponding to the onset of OAE1a (Haq et al., 1987; Gröcke et al., 1999; Gale et al., 2020), the coastal line reached the recently raised highland. The sea-level rise along the steep slope under arid climatic conditions could not provide the nutrient input to maintain the high productivity in the basin contrary to the enhanced fertilization caused by drowning of the wide lowlands. The low biotic productivity of the surface water cannot supply the sufficient volume of OM for the accumulation of TOC-rich sediments even under oxygen deficient conditions at the sea-floor (Caillaud et al., 2022).

The termination of OAE1a corresponds to the reorganization of terrestrial landscapes and climate. The coastal highland became flattened (possibly, eroded due to increased humidity) and covered in rich vegetation. Typical for the Barremian−early Aptian *Classopolis* became extinct and various Gymnospermae expanded. The wet coastal plains provided nutrient supply into the basin during the next transgressive pulse resulting in the re-entrance of normal marine biota in the early late Aptian. The PF underwent extensive bloom, nannofossil assemblage and benthic microbiota display high abundance and species diversity. The temperature of the late Aptian basin varied wildly showing a progressive cooling trend. In

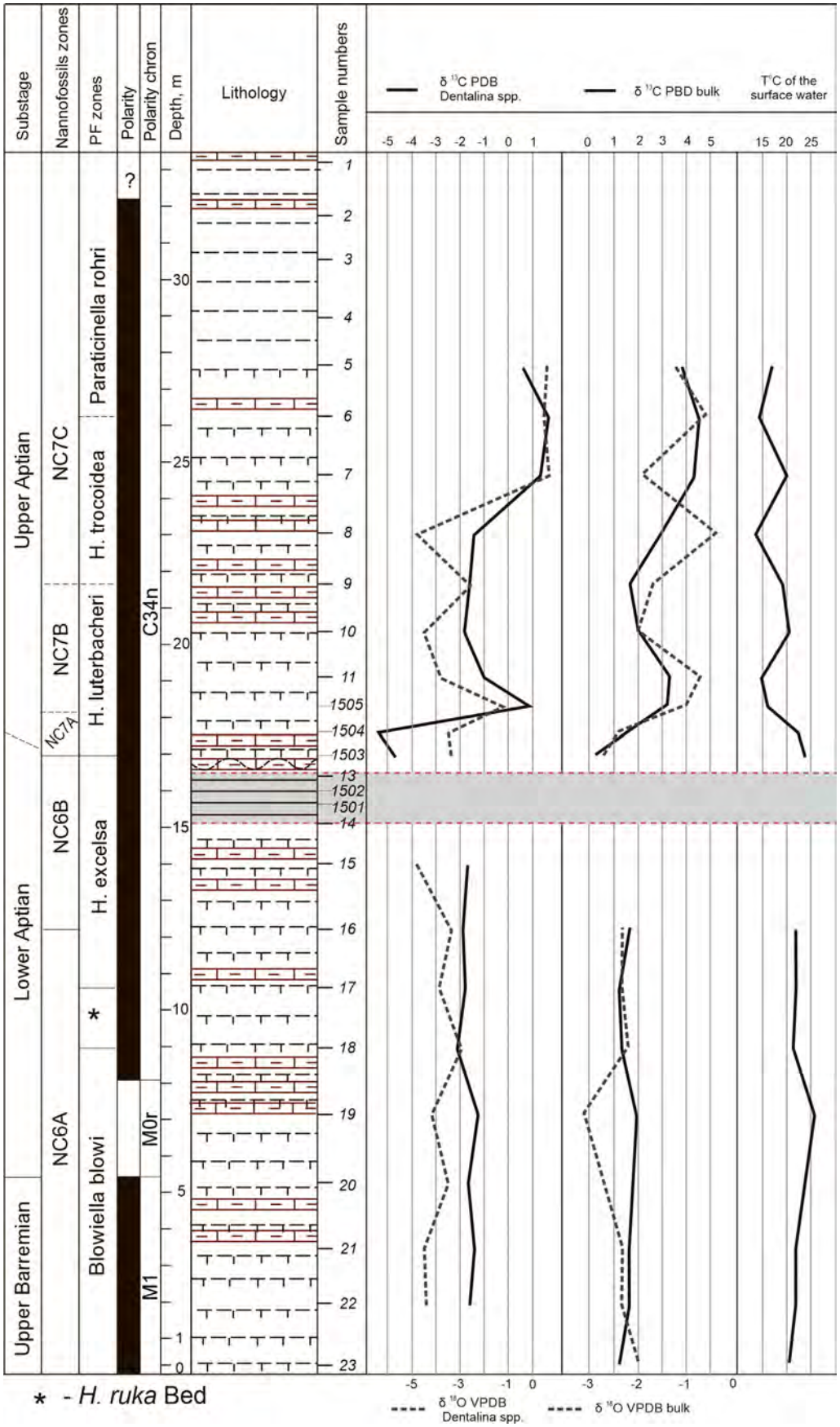

Fig. 13. $\delta^{13}C$ and $\delta^{18}O$ measured in of the *Dentalina* spp. tests and in bulk carbonate and the temperature of the surface water, calculated from $\delta^{18}O_{bulk\ carb}$.

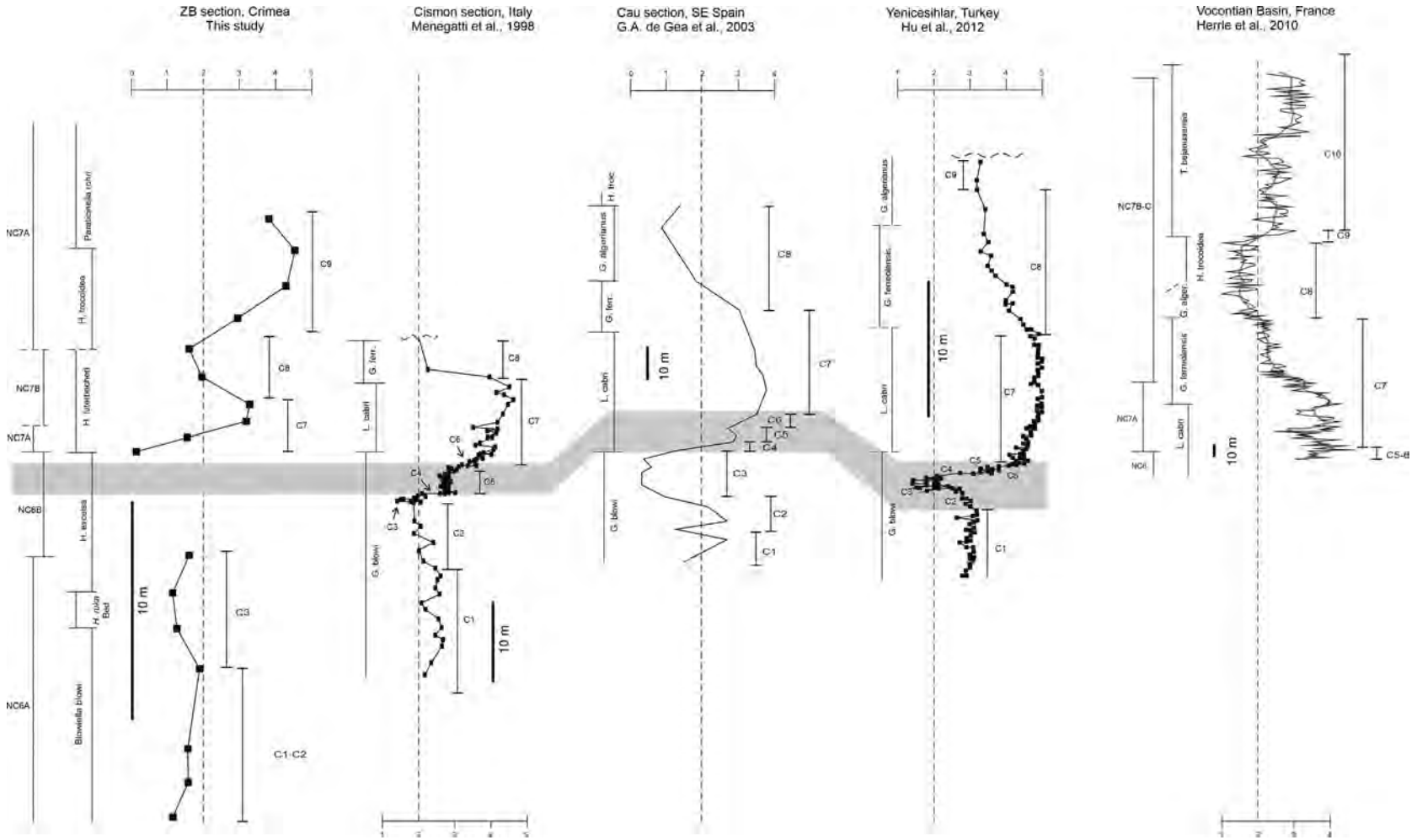

Fig. 14. Correlation of the $\delta^{13}C_{bulk}$ VPDB from ZB section to $\delta^{13}C$ curves of Italy, Spain, Turkey and France (modified from Hu et al., 2012). $\delta^{13}C$ segments are adopted from Menegatti et al. (1998).

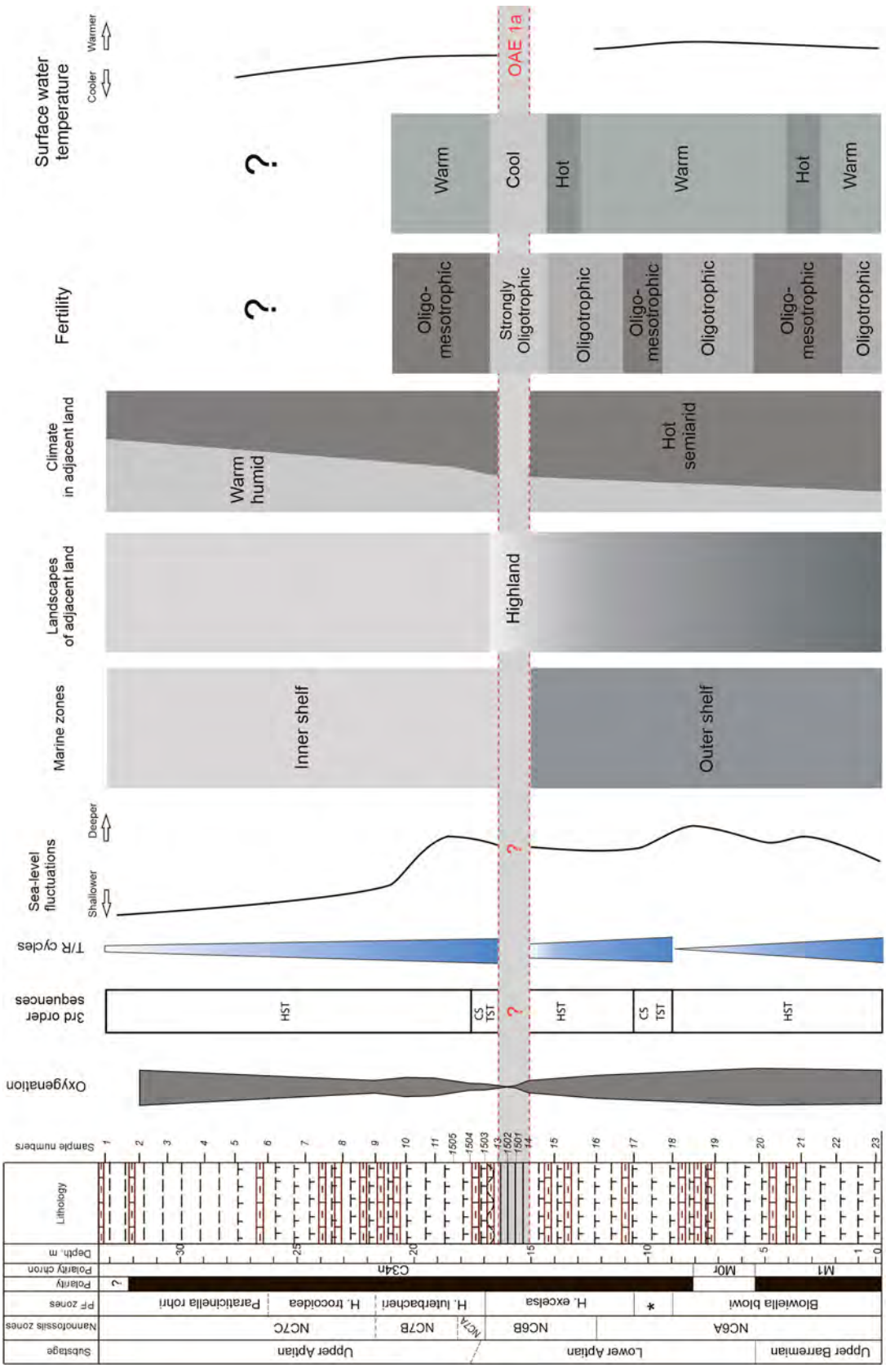

Fig. 15. Summary of the ZB section study: level of oxygenation, 3rd order sequences, T/R cycles, sea-level fluctuations, marine zones, landscapes and climate of adjacent land, fertility and temperature of surface water.

the middle of the late Aptian, a pronounced shallowing of the basin has begun, leading to a new phase in the basin evolution. The initial environmental turnovers (more likely, involving both shallowing and lower salinity) negatively affected planktonic habitat and caused dramatic decrease of PF and nannofossil total abundance and species diversity. The uppermost part of studied section lack in microfossils, but could correspond to uppermost Aptian sediments. The occurrence of fresh-water palynomorphs in this part of the section evidenced dramatic salinity drop killed marine biota and caused accumulation of low-calcareous mudrock.

5. Conclusions

The multidisciplinary study of the upper Barremian–Aptian deposits from the eastern Crimea allowed us to reveal the succession of biotic and sedimentological variation during this time span. The late Barremian to early Aptian normal hemipelagic environment underwent a strong deterioration during the global critical event OAE1a resulted in the turnover in marine biota and sedimentation. A combination of regional tectonics, climate and eustatic sea-level fluctuations caused the oligotrophy of the basin and accumulation of the specific sediments with low TOC content (lower than in embedding sediments). After the restoration of the normal marine environment after the OAE1a(?), the basin was repopulated by new microplanktonic and microbenthic communities simultaneously with landscape deterioration in the adjacent territories. These dramatic changes evidence a strong impact associated with OAE1a phenomena in this part of the wide Crimean-Caucasus basin.

Data availability

Data will be made available on request.

Acknowledgments

This study was funded by research project N№ 21-77-00081 of the Russian Science Foundation (M. Karpuk) and was carried out following the plans of the scientific research of the Geological Institute of RAS (E. Shcherbinina, E. Shchepetova, G. Aleksandrova, B. Pokrovsky, I. Latysheva), of the Trofimuk Institute of Petroleum Geology and Geophysics of SB RAS (L. Glinskikh) Authors would like to thank I. Byakin for his help in collecting samples. Also, we are grateful to V.A. Drits and E.V. Pokrovskaya for their assistance in the interpretation of XRD-profiles. We would also like to express our deep gratitude to both reviewers and Associated Editor Elena Yazykova for their useful and significant comments.

References

Abbink, O.A., Targarona, J., Brinkhuis, H., Visscher, H., 2001. Late Jurassic to earliest Cretaceous palaeoclimatic evolution of the Southern North Sea. Global and Planetary Change 30, 231–256.

Abbink, O.A., Van Konijnenburg-Van Cittert, J.H.A., Visscher, H., 2004. A sporomorph ecogroup model for the Northwest European Jurassic–Lower Cretaceous: concepts and framework. Netherlands Journal of Geosciences 83 (1), 17–38.

Aguado, R., Company, M., O'Dogherty, L., Sandoval, J., Tavera, J.M., 1992. Biostratigraphic analysis of the pelagic Barremian/Aptian in the Betic Cordillera (southern Spain): preliminary data. Cretaceous Research 13, 445–452.

Aguado, R., Castro, J.M., Company, M., de Gea, G.A., 1999. Aptian bio-events – an integrated biostratigraphic analysis of the Almadich Formation, Inner Prebetic Domain, SE Spain. Cretaceous Research 20, 663–683.

Aguado, R., de Gea, G.A., Castro, J.M., O'Dogherty, L., Quijano, M.L., Naafs, B.D.A., Pancost, R.D., 2014. Late Barremian–early Aptian dark facies of the Subbetic (Betic Cordillera, southern Spain): Calcareous nannofossil quantitative analyses, chemostratigraphy and palaeoceanographic reconstructions. Palaeogeography, Palaeoclimatology, Palaeoecology 395, 198–221.

Aguado, R., Reolid, M., Molina, E., 2018. Response of calcareous nannoplankton to the Late Cretaceous Oceanic Anoxic Event 2 at Oued Bahloul (central Tunisia). Palaeogeography, Palaeoclimatology, Palaeoecology 459, 289–305.

Alvin, K.L., 1982. Cheirolepidiaceae: biology, structure and paleoecology. Review of Palaeobotany and Palynology 37, 71–98.

Amorosi, A., 1995. Glaucony and sequence stratigraphy; a conceptual framework of distribution in siliciclastic sequences. Journal of Sedimentary Research 65 (4b), 419–425. https://doi.org/10.1306/D4268275-2B26-11D7-8648000102C1865D.

Amorosi, A., 2013. The occurrence of glaucony in the stratigraphic record: distribution patterns and sequence-stratigraphic significance. Linking diagenesis to sequence stratigraphy 37–53.

Andreau, B., 1992. Associations d'ostracodes et paleoecologie du Cretace (Barremien a Turonien) le long d'une transversal Agadir-Nador (Maroc). Palaeogeography, Palaeoclimatology, Palaeoecology 99, 291–319.

Anfimova, G., 2015. State of the art and problems of the lower Cretaceous formation stratotypes and key sections of the Mountain Crimea. Geologia 2 (69), 17–23 (in Russian).

Astakhova, T.V., Gorak, S.V., Kraeva, E.Ya., 1984. Geology of Ukrainian Shelf. Stratigraphy (Shelf and Black Sea Nearshore). Naukova Dumka, Kiev, p. 184 (in Russian).

Avram, E., Drăgănescu, A., Szasz, L., Neagu, Th., 1988. Stratigraphy of the outcroping Cretaceous deposits in the Southern Dobrogea (SE Romania). Mémoirii Institut si Géologie et de Géophysica 33, 5–34.

Baraboshkin, E. Yu., 2005. Early Cretaceous paleogeography of the East European Platform and its southern border. In: Morozov, A.F. (Ed.), 400 Ma of the geological history of the Russia. Moscow, Geokart, pp. 201–232 (in Russian).

Baraboshkin, E.Yu., Guzhikov, A.Yu., Mutterlose, J., Yampolskaya, O.B., Pimenov, M.V., Gavrilov, S.S., 2004. New data on stratigraphy of the Barremian-Aptian deposits of the Crimean Mountains due to detection of the chron M0 analogue in Verkhorechie section. In: Seria 4. Geology, vol. 1. Vestnik of Moscow University, pp. 10–20 (in Russian).

Barragan, R., Melinte, M.C., 2006. Palaeoenvironmental and palaeobiologic changes across the Barremian/Aptian boundary interval in the Tethys Realm, Mexico and Romania. Cretaceous Research 27, 529–541.

Barron, E.J., 1983. A warm, equable Cretaceous: The nature of the problem. Earth-Science Reviews 19, 305–338.

Bellanca, A., Erba, E., Neri, R., Premoli Silva, I., Sprovieri, M., Tremolada, F., Verga, D., 2002. Palaeoceanographic significance of the Tethyan 'Livello Selli' (Early Aptian) from the Hybla Formation, northwestern Sicily: biostratigraphy and high-resolution chemostratigraphic records. Palaeogeography, Palaeoclimatology, Palaeoecology 185, 175–196.

Benenson, V.A., 1985. Lower Cretaceous of the South of USSR. Nauka, Moscow, p. 224.

Benson, R.H., 1984. Estimating greater paleodepths with Ostracodes, especially in past thermospheric oceans. Palaeogeography, Palaeoclimatology, Palaeoecology 48, 107–141.

Bonin, A., Pucéat, E., Vennin, E., Mattioli, E., Aurell, M., Joachimski, M., Barbarin, N., Laffont, R., 2016. Cool episode and platform demise in the Early Aptian: new insights on the links between climate and carbonate production. Paleoceanography 31, 66–80.

Bottini, C., Erba, E., 2018. Mid-Cretaceous paleoenvironmental changes in the western Tethys. Climate of the Past 14, 1147–1163. https://doi.org/10.5194/cp-14-1147-2018.

Bottini, C., Mutterlose, J., 2012. Integrated stratigraphy of Early Aptian black shales in the Boreal Realm: calcareous nannofossil and stable isotope evidence for global and regional processes. Newsletters on Stratigraphy 45, 115–137.

Bottini, C., Cohen, A.S., Erba, E., Jenkyns, H.C., Coe, A.L., 2012. Osmium-isotope evidence for volcanism, weathering, and ocean mixing during the early Aptian OAE1a. Geology 40 (7), 583–586.

Bottini, C., Erba, E., Tiraboschi, D., Jenkyns, H.C., Schouten, S., Sinninghe Damsté, J.S., 2015. Climate variability and ocean fertility during the Aptian Stage. Climate of the Past 11, 383–402.

Bown, P.R., Young, J.R., 1998. Techniques. In: Bown, P.R. (Ed.), Calcareous Nannofossil Biostratigraphy. Chapman & Hall, London, pp. 16–28.

Bralower, 1988. Calcareous nannofossil biostratigraphy and assemblages of the Cenomanian-Turonian boundary interval: implications for the origin and timing of oceanic anoxia. Paleoceanography 3, 275–316.

Bralower, T.J., Sliter, W.V., Arthur, M.A., Leckie, R.M., Allard, D.J., Schlanger, S.O., 1993. Dysoxic/anoxic episodes in the Aptian-Albian (Early Cretaceous). In: Pringle, M., Sager, W.W., Sliter, W.V., Stein, S. (Eds.), The Mesozoic Pacific: Geology, Tectonics and Volcanism, Geoph. Monog. Series, vol. 77. American Geophysical Union, Washington, D. C., pp. 5–37

Bralower, T.J., Arthur, M.A., Leckie, R.M., Sliter, W.V., Allard, D.J., Schlanger, S.O., 1994. Timing and palaeoceanography of oceanic dysoxia/anoxia in the late Barremian to early Aptian (early Cretaceous). PALAIOS 9, 335–369.

Briggs, D.J., 1977. Soils. Butterworth, London, p. 192.

Brovina, E.A., 2017. Planktonic foraminiferal biostratigraphy of the upper Barremian and Aptian of Crimea. Stratigraphy and Geological Correlation 25 (5), 515–531.

Brovina, E.A., Karpuk, M.S., Shcherbinina, E.A., Tesakova, E.M., 2017. Stratigraphy of the Aptian sediments of Alma R. basin based on new micropaleontological data. Bulleten MOIP. Otdel Geologii 6, 26–42 (in Russian).

Caillaud, A., Quijada, M., Hlohowskyj, S.R., Chappaz, A., Bout-Roumazeilles, V., Reynaud, J.-Y., Riboulleau, A., Baudin, F., Adatte, T., Ferry, J.-N., Tribovillard, N., 2022. Assessing controls on organic matter enrichments in hemipelagic marls of the Aptian-Lower Albian Blue Marls of the Vocontian Basin (France): an unexpected variability observed from multiple "organic-rich" levels. Earth Sciences Bulletin, 200051. https://doi.org/10.1051/bsgf/2022001.

Chaloner, W.G., 1958. The Carboniferous upland flora. Geological Magazine 95 (3), 261–262.

Channell, J.E.T., Erba, E., Muttoni, G., Tremolada, F., 2000. Early Cretaceous Magnetic Stratigraphy in the APTICORE Drill Core and Adjacent Outcrop at Cismon (Southern Alps, Italy), and the Correlation to the Proposed Barremian/Aptian Boundary Stratotype, vol. 112. Geological Society of America, Bulletin, pp. 1430–1443.
Coccioni, R., Erba, E., Premoli Silva, I., 1992. Barremian-Aptian calcareous plankton biostratigraphy from the Gorgo a Cerbara section (Marche, Central Italy) and implications for plankton evolution. Cretaceous Research 13, 517–537.
Coccioni, R., Marsili, A., Luciani, V., 2006. Cretaceous oceanic anoxic events and radially elongated chambered planktonic foraminifera: paleoecological and paleoceanographic implications. Palaeogeography, Palaeoclimatology, Palaeoecology 235, 66–92.
Cogley, J.G., Aikman, M., 1997. The insoluble residue test for abundance of carbonate. Earth Surface Processes and Landforms: The Journal of the British Geomorphological Group 22 (11), 1053–1059.
Colpaert, C., Nikitenko, B.L., Khafaeva, S.N., 2017. Stratigraphy and ecostratigraphic distribution of foraminiferal morphogroups from the Upper Jurassic of the Makar'yev section (Unzha River, Volga River basin). Russian Geology and Geophysics 58 (1), 70–86. https://doi.org/10.1016/j.rgg.2016.04.014.
de Gea, G.A., Castro, J.M., Aguado, R., Ruiz-Ortiz, P.A., Company, M., 2003. Lower Aptian carbon isotope stratigraphy from a distal carbonate shelf setting: the Cau section, Prebetic zone, SE Spain. Palaeogeography, Palaeoclimatology, Palaeoecology 200 (1–4), 207–219. https://doi.org/10.1016/S0031-0182(03)00451-6.
Deconinck, J.F., Hesselbo, S.P., Debuisser, N., Averbuch, O., Baudin, F., Bessa, J., 2003. Environmental controls on clay mineralogy of an Early Jurassic mudrock (Blue Lias Formation, southern England). International Journal of Earth Sciences 92 (2), 255–266. https://doi.org/10.1007/s00531-003-0318-y.
Deconinck, J.F., Boué, D., Amédro, F., Baudin, F., Bruneau, L., Huret, E., Landrein, P., Moreau, J.-D., Santoni, A.L., 2021. First record of early Aptian Oceanic Anoxic Event 1a from the Paris Basin (France)-Climate signals on a terrigenous shelf. Cretaceous Research 125, 104846.
Des Marais, D.J., 2001. Isotope evolution of the biogeochemical carbon cycle during the Precambrian. Reviews in Mineralogy and Geochemistry 43 (1), 555–578.
Donze, P., 1975. Tethysia, nouveau genre d'Ostracode bathyal du jurassique superieur e cretace inferieur mesogeen. Geobios 8 (3), 185–190.
Dragastan, O.N., Antoniade, C., Stoica, M., 2014. Biostratigraphy and zonation of the Lower Cretaceous carbonate succession from Cernavodă-lock section, South Dobrogea, eastern part of the Moesian Platform (Romania). Carpathian Journal of Earth and Environmental Sciences 9 (1), 231–260.
Drits, V.A., Sakharov, B.A., 1976. X-ray Analysis of Mixed-Layer Minerals. Nauka, Moscow, p. 256.
Drits, V.A., Tchoubar, C., 1990. X-Ray Diffraction by Disordered Lamellar Structures. Springer-Verlag, Heidelberg, p. 371. https://doi.org/10.1007/978-3-642-74802-8.
Dumitrescu, M., Brassell, S.C., 2006. Compositional and isotopic characteristics of organic matter for the early Aptian oceanic anoxic event at Shatsky Rise, ODP leg 198. Palaeogeography, Palaeoclimatology, Palaeoecology 235, 168–191.
Duuc, I., 2002. Middle Cretaceous Palaeophytogeography of the Central Tethys and Geodynamic Implications.
Epstein, S., Buchsbaum, R., Lowenstam, H.A., Urey, H.C., 1953. Revised carbonate-water temperature scale. Geological Society of America Bulletin 62, 417–426.
Erba, E., 1992. Calcareous nannofossil distribution in pelagic rhythmic sediments (Aptian–Albian Piobbico core, central Italy). Rivista Italiana di Paleontologia e Stratigrafia 97, 455–484.
Erba, E., 1994. Nannofossils and superplumes: the early Aptian nannoconid crisis. Paleoceanography 9, 483–501.
Erba, E., Tremolada, F., 2004. Nannofossil carbonate fluxes during the Early Cretaceous: Phytoplankton response to nutrification episodes, atmospheric CO2, and anoxia. Paleoceanography 19, 1–18.
Erba, E., Premoli-Silva, I., Watkins, D.K., 1995. Cretaceous calcareous plankton biostratigraphy of sites 872 through 879. In: Proc. of the Ocean Drilling Program, Scientific Results, vol. 144, pp. 157–169.
Erba, E., Bottini, C., Weissert, H., Keller, C.E., 2010. Calcareous nannoplankton response to surface-water acidification around Oceanic Anoxic Event 1a. Science 329, 428–432. https://doi.org/10.1126/science.1188886.
Erba, E., Duncan, R.A., Bottini, C., Tiraboschi, D., Weissert, H., Jenkyns, H.C., Malinverno, A., 2015. Environmental Consequences of Ontong Java Plateau and Kerguelen Plateau Volcanism. In: The origin, Evolution, and Environmental Impact of Oceanic Large Igneous Provinces, vol. 511. Geological Society of America Special Paper, pp. 271–303. https://doi.org/10.1130/2015.2511(15.
Erba, E., Bottini, C., Faucher, G., Gambacorta, G., Visentin, S., 2019. The response of calcareous nannoplankton to Oceanic Anoxic Events: The Italian pelagic record. Bollettino della Societa Paleontologica Italiana 58 (1), 51–71.
Espitalie, J., Bordenave, M.L., 1993. Rock-Eval pyrolysis. In: Bordenave, M.L. (Ed.), Applied Petroleum Geochemistry, Technip ed., pp. 237–361 Paris.
Espitalié, J., Deroo, G., Marquis, F., 1985. Rock-Eval pyrolysis and its applications. Revue de l'Institut Français du Petrole 40 (5), 563–579. https://doi.org/10.2516/ogst:1986003.
Filatov, O.M., 1961. Morphology and evolution of the structural formations in the southeastern Crimea. Sovetskaya Geologia 2, 92–107 (in Russian).
Fisher, C.G., Hay, W.W., 1999. Calcareous nannofossils as indicators of mid-Cretaceous paleofertility along an ocean front, U.S. Western Interior. In: Barrera, E., Johnson, C.C. (Eds.), Evolution of the Cretaceous Ocean-Climate System, Geological Society of America Special Paper, vol. 332. Colorado, Boulder, pp. 161–169.
Föllmi, K.B., 2012. Early Cretaceous life, climate and anoxia. Cretaceous Research 35, 230–257.
Föllmi, K.B., 2016. Sedimentary condensation. Earth-Science Reviews 152, 143–180. https://doi.org/10.1016/j.earscirev.2015.11.016.
Francis, J.E., 1983. The dominant conifer of the Jurassic Purbeck Formation, England. Palaeontology (2), 277–294.
Friedrich, O., Erbacher, J., Mutterlose, J., 2006. Paleoenvironmental changes across the Cenomanian/Turonian Boundary Event (Oceanic Anoxic Event 2) as indicated by benthic foraminifera from the Demerara Rise (ODP Leg 207). Revue de Micropaleontologie 49, 121–139.
Friedrich, O., Norris, R.D., Erbacher, J., 2012. Evolution of middle to Late Cretaceous oceans—a 55 m.y. record of Earth's temperature and carbon cycle. Geology 40 (2), 107–110.
Fu, X., Wang, J., Wend, H., Wang, Z., Zeng, S., Song, C., Wang, D., Nie, Y., 2020. Carbon-isotope record and paleoceanographic changes prior to the OAE1a in the Eastern Tethys: Implication for the accumulation of organic-rich sediments. Marine and Petroleum Geology 113, 104049.
Gale, A.S., Mutterlose, J., Batenburg, S., 2020. Cretaceous period. Carbon isotope stratigraphy. In: Gradstein, F.M., Ogg, J.G., Schmitz, M.D., Ogg, G.M. (Eds.), The Geologic Time Scale, vol. 1. Elsevier, Boston, pp. 309–344. Ch. 11.
Gavrilov, Yu.O., Shchepetova, E.V., Baraboshkin, E.Y., Shcherbinina, E.A., 2002. The Early Cretaceous anoxic basin of the Russian Plate: sedimentology and geochemistry. Lithology and Mineral Resources 37 (4), 310–329.
Gibbs, R.J., 1977. Clay mineral segregation in the marine environment. Journal of Sedimentary Research 47 (1), 237–243. https://doi.org/10.1306/212F713A-2B24-11D7-8648000102C1865D.
Giraud, F., Pittet, B., Grosheny, D., Baudin, F., Lécuyer, C., Sakamoto, T., 2018. The palaeoceanographic crisis of the Early Aptian (OAE 1a) in the Vocontian Basin (SE France). Palaeogeography, Palaeoclimatology, Palaeoecology 511, 483–505.
Godet, A., Bodin, S., Adatte, T., Föllmi, K.B., 2008. Platform-induced clay-mineral fractionation along a northern Tethyan basin-platform transect: implications for the in- terpretation of Early Cretaceous climate change (Late Hauterivian-Early Aptian). Cretaceous Research 29 (5–6), 830–847. https://doi.org/10.1016/j.cretres.2008.05.028.
Gorbachik, T.N., 1986. Jurassic and Early Cretaceous Planktonic Foraminifera of the South of USSR. Nauka, Moskva, p. 239 (in Russian).
Gorbachik, T.N., Yanin, B.T., 1972. Aptian-Albian Deposits of Alma – Salgir Interstream Area (Crimea) and Their Stratification Using Foraminifera. In: Seria 4. Geology, vol. 2. Vestnik Moscow University, pp. 64–72 (in Russian).
Gozhik, P.F., 2013. Stratigraphy of Upper Proterozoic to Phanerozoic of the Ukraine. Logos, Kyiv, p. 637 (in Ukrainian).
Gröcke, D.R., Hesselbo, S.P., Jenkyns, H.C., 1999. Carbon-isotope composition of Lower Cretaceous fossil wood: ocean-atmosphere chemistry and relation to sea-level change. Geology 27 (2), 155–158.
Grossman, E.L., Joachimski, M.M., 2020. Oxygen isotope Stratigraphy. In: Gradstein, F.M., Ogg, J.G., Schmitz, M.D., Ogg, G.M. (Eds.), The Geologic Time Scale, vol. 1. Elsevier, Boston, pp. 279–307. Ch. 10.
Hallam, A., 1985. A review of Mesozoic climates. Journal of the Geological Society 142 (3), 433–445.
Haq, B.U., Hardenbol, J.A.N., Vail, P.R., 1987. Chronology of fluctuating sea levels since the Triassic. Science 235 (4793), 1156–1167.
Hart, M.B., Crittenden, S., 1985. Early Cretaceous Ostracoda from the Goban Spur; D.S.D.P. leg 80, Site 549. Cretaceous Research 6, 219–233.
Heimhofer, U., Hochuli, P.A., Herrle, J.O., Weissert, H., 2006. Contrasting origins of Early Cretaceous black shales in the Vocontian basin: Evidence from palynological and calcareous nannofossil records. Palaeogeography, Palaeoclimatology, Palaeoecology 235, 93–109.
Heldt, M., Mutterlose, J., Berner, U., Erbacher, J., 2012. First high-resolution δ13C-records across black shales of the Early Aptian Oceanic Anoxic Event 1a within the mid-latitudes of northwest Europe (Germany, Lower Saxony Basin). Newsletters on Stratigraphy 45 (2), 151–169.
Herman, A.B., Spicer, R.A., 2010. Mid-Cretaceous floras and climate of the Russian high Arctic (Novosibirsk Islands, northern Yakutiya). Palaeogeography, Palaeoclimatology, Palaeoecology 295 (3–4), 409–422.
Herrle, J.O., Mutterlose, J., 2003. Calcareous nannofossils from the Aptian-early Albian of SE France: paleoecological and biostratigraphic implications. Cretaceous Research 24, 1–22.
Herrle, J.O., Pross, J., Friedrich, O., Köβler, P., Hemleben, C., 2003. Forcing mechanisms for mid-Cretaceous black shale formation: evidence from the Upper Aptian and Lower Albian of the Vocontian Basin (SE France). Palaeogeography, Palaeoclimatology, Palaeoecology 190, 399–426.
Herrle, J.O., Kosler, P., Bollmann, J., 2010. Palaeoceanographic differences of early Late Aptian black shale events in the VocontianBasin (SE France). Palaeogeography, Palaeoclimatology, Palaeoecology 297, 367–376.
Hu, X., Zhao, K., Yilmaz, I.O., Li, Y., 2012. Stratigraphic transition and palaeoenvironmental changes from the Aptian oceanic anoxic event 1a (OAE1a) to the oceanic red bed 1 (ORB1) in the Yenicesihlar section, central Turkey. Cretaceous Research 38, 40–51.
Huber, B.T., Hodell, D.A., Hamilton, C.P., 1995. Middle–late Cretaceous climate of the southern high latitudes: Stable isotopic evidence for minimal equator-to-pole thermal gradients. Geological Society of America Bulletin 107, 1164–1191.
Jaillard, E., Kassab, W.H., Giraud, F., Robert, E., Masrour, M., Bouchaou, L., El Hariri, Kh, Hammed, M.S., Aly, M.F., 2019. Aptianeearly Albian sedimentation in the Essaouira-Agadir basin, Western Morocco. Cretaceous Research 102, 59–80.

Jenkyns, H.C., 1980. Cretaceous anoxic events: from continents to oceans. Journal of the Geological Society 137, 171–188.
Jenkyns, H.C., 2003. Evidence for rapid climate change in the Mesozoic- Palaeogene greenhouse world. Philosophical Transactions of the Royal Society of London,Series A: Mathematical, Physical and Engineering Sciences 361 (1810), 1885–1916.
Jenkyns, H.C., Forster, A., Schouten, S., Sinninghe Damste, J.S., 2004. High temperatures in the late Cretaceous Arctic Ocean. Nature 432, 888–892.
Kanungo, S., Bown, P.R., Young, J.R., Gale, A.S., 2018. A brief warming event in the late Albian: evidence from calcareous nannofossils, macrofossils, and isotope geochemistry of the Gault Clay Formation, Folkestone, southeastern England. Journal of Micropalaeontology 37, 231–247.
Karpuk, M., 2021. Relative depth reconstruction method using marine ostracods: a case study from the upper Barremian-Aptian of the Crimean Mountains. Cretaceous Research 120 104719. https://doi.org/10.1016/j.cretres.2020.104719.
Karpuk, M.S., Tesakova, E.M., 2013. New Ostracods of the Family Cytheruridae G. Mueller from the Barremian–Albian of the Southwestern Crimea. Paleontological Journal 47 (6), 588–596.
Karpuk, M.S., Tesakova, E.M., 2014. New Ostracodes of the families Loxoconchidae and Trachyleberididae from the Barremian–Albian of Southwestern Crimea. Paleontological Journal 48 (2), 177–181.
Karpuk, M.S., Shcherbinina, E.A., Brovina, E.A., Aleksandrova, G.N., Guzhikov, A.Yu., Shchepetova, E.V., Tesakova, E.M., 2018. Integrated stratigraphy of the Upper Barremian–Aptian sediments from the south-eastern Crimea. Geologica Carpathica 69 (5), 498–511. https://doi.org/10.1515/geoca-2018-0029.
Keller, C.E., Hochuli, P.A., Weissert, H., Bernasconi, S.M., Giorgioni, M., Garcia, T.I., 2011. A volcanically induced climate warming and floral change preceded the onset of OAE1a (Early Cretaceous). Palaeogeography, Palaeoclimatology, Palaeoecology 305 (1–4), 43–49.
Kroopnick, P.M., 1985. The distribution of ^{13}C of $\sum CO_2$ in the world oceans. Deep-Sea Research 32 (1), 57–84.
Kuhnt, W., Holbourn, A., Moullade, M., 2011. Transient global cooling at the onset of early Aptian oceanic anoxic event (OAE) 1a. Geology 39 (4), 323–326.
Langford, F.F., Blanc-Valleron, M.M., 1990. Interpreting Rock-Eval pyrolysis data using graphs of pyrolizable hydrocarbons vs. total organic carbon. AAPG Bulletin 74 (6), 799–804.
Leckie, R.M., 1987. Paleoecology of mid-Cretaceous planktonic foraminifera: a comparison of open ocean and epicontinental sea assemblages. Micropaleontology 164–176.
Leckie, R.M., 1989. A paleoceanographic model for the early evolutionary history of planktonic Foraminifera. Palaeogeography, Palaeoclimatology, Palaeoecology 73, 107–138.
Leckie, R.M., Bralower, T.J., Cashman, R., 2002. Oceanic anoxic events and plankton evolution: biotic response to tectonic forcing during the mid-Cretaceous. Paleoceanography 17, 1–29.
Leeder, M.R., 1982. Sedimentology. Process and Product. Sedimentology Process and Product. Departement of Earth Sciences, University of Leeds, p. 344.
Lees, J.A., Bown, P.R., Mattioli, E., 2005. Problems with proxy? Cautonary tales of calcareous nannofossil paleoenvironmental indicators. Micropaleontology 51 (4), 333–343.
Lubke, N., Mutterlose, J., 2016. The impact of OAE1a on marine biota deciphered by size variations of coccoliths. Cretaceous Research 61, 169–179.
Luciani, V., Cobianchi, M., Jenkyns, H.C., 2001. Biotic and geochemical response to anoxic events: the Aptian pelagic succession of the Gargano Promontory (southern Italy). Geological Magazine 138 (3), 277–298.
Mackensen, A., Schmiedl, G., 2019. Stable carbon isotopes in paleoceanography: atmosphere, oceans, and sediments. Earth-Science Reviews 197, 102893. https://doi.org/10.1016/j.earscirev.2019.102893.
Mackensen, A., Hubberten, H.W., Bickert, T., Fischer, G., Fütterer, D.K., 1993. The $\delta^{13}C$ in benthic foraminiferal tests of Fontbotia wuellerstorfi (Schwager) relative to the $\delta^{13}C$ of dissolved inorganic carbon in Southern ocean deep water: implications for glacial ocean circulation models. Paleoceanography 8 (5), 587–610.
Matveev, A.V., 2016. Calcareous Nannofossils of the Cretaceous of Southern Slope of Ukrainian Shield and Its Southern Frame (Ph.D. thesis). Kharkov National University, p. 380 (in Russian).
McAnena, A., Flögel, S., Hofmann, P., Herrle, J.O., Griesand, A., Pross, J., Talbot, H.M., Rethemeyer, J., Wallmann, K., Wagner, T., 2013. Atlantic cooling associated with a marine biotic crisis during the mid-Cretaceous period. Nature Geosciences 6 (7), 558–561.
Méhay, S., Keller, C.E., Bernasconi, S.M., Weissert, H., Erba, E., Bottini, C., Hochuli, P.A., 2009. A volcanic CO_2 pulse triggered the Cretaceous Oceanic Anoxic Event1a and a biocalcification crisis. Geology 37 (9), 819–822.
Melinte, M., Mutterlose, J., 2001. A Valanginan (Early Cretaceous) 'boreal nannoplankton excursion' in sections from Romania. Marine Micropaleontology 43, 1–25.
Menegatti, A.P., Weissert, H., Brown, R.S., Tyson, R.V., Farrimond, P., Strasser, A., Caron, M., 1998. High-resolution $\delta^{13}C$ stratigraphy through the early Aptian Livello Selli of the Alpine Tethys. Paleoceanography 13, 530–545.
Moore, D.M., Reynolds, R.C., 1997. X-ray Diffraction and Identification and Analysis of Clay Minerals, second ed. Oxford University Press, New York, p. 378pp.
Muratov, M.V., 1973. Geology of the Crimean Peninsula. Moscow, p. 192 (in Russian).
Mutterlose, J., Bornemann, A., Herrle, J.O., 2005. Mesozoic calcareous nannofossils – state of the art. Paläontologische Zeitschrift 79 (1), 113–133.
Naafs, B.D.A., Pancost, R.D., 2016. Sea-surface temperature evolution across Aptian Oceanic Anoxic Event 1a. Geology 44, 959–962.
Nagy, J., 1992. Environmental significance of foraminiferal morphogroups in Jurassic North Sea deltas. Palaeogeography, Palaeoclimatology, Palaeoecology 95 (1–2), 111–134.
Nikishin, A.M., Okay, A., Tüysüz, O., Demirer, A., Wannier, M., Amelin, N., Petrov, E., 2015a. The Black Sea basins structure and history: New model based on new deep penetration regional seismic data. Part 2: tectonic history and paleeogography. Marine and Petroleum Geology 59, 656–670.
Nikishin, A.M., Wannier, M., Alekseev, A.S., Almendinger, O.A., Fokin, P.A., Gabdullin, R.R., Khudoley, A.K., Kopaevich, L.F., Mityukova, A.V., Petrov, E.I., Rubtsova, E.V., 2015b. Mesozoic to recent geological history of southern Crimea and the Eastern Black Sea region. In: Sosson, M., Stephenson, R.A., Adamia, S.A. (Eds.), Tectonic Evolution of the Eastern Black Sea and Caucasus. Geological Society, London, Special Publications, p. 428. https://doi.org/10.1144/SP428.1.
Nikitenko, B., Reolid, M., Glinskikh, L., 2013. Ecostratigraphy of benthic foraminifera for interpreting Arctic record of Early Toarcian biotic crisis (Northern Siberia, Russia). Palaeogeography, Palaeoclimatology, Palaeoecology 376, 200–212.
Norris, R.D., Bice, K.L., Magno, E.A., Wilson, P.A., 2002. Jiggling the tropical thermostat in the Cretaceous hothouse. Geology 30, 299–302.
O'Brien, C.L., Robinson, S.A., Pancost, R.D., SinninghеDamsté, J.S., Schoulten, S., Lunt, D.J., Alsenz, H., Bornemann, A., Bottini, C., Brassell, S.C., Farnsworth, A., Forster, A., Huber, B.T., Inglis, G.N., Jenkyns, H.C., Linnert, C., Littler, K., Markwick, P., McAnena, A., Mutterlose, J., Naafs, B.D.A., Püttmann, W., Sluijs, A., van Helmond, N.A.G.M., Vellekoop, J., Wagner, T., Wrobel, N.E., 2017. Cretaceous sea-surface temperature evolution: constraints from TEX 86 and planktonic foraminiferal oxygen isotopes. Earth-Science Reviews 172, 224–247.
O'Connor, L.K., Robinson, S.A., Naafs, B.D.A., Jenkyns, H.C., Henson, S., Clarke, M., Pancost, R.D., 2019. Late Cretaceous temperature evolution of the southern high latitudes: A TEX86 perspective. Paleoceanography and Paleoclimatology 34. https://doi.org/10.1029/2018PA003546.
Odin, G.S., 1988. Green Marine Clays: Oolitic Ironstone Facies, Verdine Facies, Glaucony Facies and Celadonite-Bearing Rock Facies – A Comparative Study. Developments in Sedimentology 45, 471. Elsevier, Amsterdam.
Pagani, M., Huber, M., Sageman, B., 2014. Greenhouse Climates. Treatise Geochem 37, 281–304.
Pancost, R.D., Crawford, N., Magness, S., Turner, A., Jenkyns, H.C., Maxwell, J.R., 2004. Further evidence for the development of photic-zone euxinic conditions during Mesozoic oceanic anoxic events. Journal of the Geological Society 161, 353–364.
Patruno, S., Triantaphyllou, M.V., Erba, E., Dimiza, M.D., Bottini, C., Kaminski, M.A., 2015. The Barremian and Aptian stepwise development of the 'Oceanic Anoxic Event 1a'(OAE1a) crisis: Integrated benthic and planktic high-resolution palaeoecology along the Gorgo a Cerbara stratotype section (Umbria–Marche Basin, Italy). Palaeogeography, Palaeoclimatology, Palaeoecology 424, 147–182.
Peybernes, C., Giraud, F., Jaillard, E., Robert, E., Masrour, M., Aoutem, M., Içame, N., 2013. Stratigraphic framework and calcareous nannofossil productivity of the Essaouira-Agadir Basin (Morocco) during the Aptian–Early Albian: Comparison with the north-Tethyan margin. Cretaceous Research 39, 149–169.
Philippe, M., Barbacka, M., Gradinaru, E., Iamandei, E., Iamandei, S., Kázmér, M., Popa, M., Szakmány, G., Tchoumatchenco, P., Zatoń, M., 2006. Fossil wood and Mid-Eastern Europe terrestrial palaeobiogeography during the Jurassic–Early Cretaceous interval. Review of Palaeobotany and Palynology 142 (1–2), 15–32.
Quijano, M.K., Castro, J.M., Pancost, R.D., de Gea, G.A., Najarro, M., Aguado, R., Rosales, I., Martín-Chivelet, J., 2012. Organic geochemistry, stable isotopes, and facies analysis of the Early Aptian OAE – New records from Spain (Western Tethys). Palaeogeography, Palaeoclimatology, Palaeoecology 365, 276–293.
Rateev, M.A., 1964. Regularities in the Distribution and Genesis of Clay Minerals in Recent and Old Marine Basin. In: Transactions Geological Institute of Academy of Sciences of the USSR, vol 112. Nauka, Moscow, p. 274 (In Russian).
Reolid, M., Rodríguez-Tovar, F.J., Nagy, J., Olóriz, F., 2008. Benthic foraminiferal morphogroups of mid to outer shelf environments of the Late Jurassic (Prebetic Zone, southern Spain): characterisation of biofacies and environmental significance. Palaeogeography, Palaeoclimatology, Palaeoecology 261, 280—299.
Reolid, M., Nagy, J., Rodríguez-Tovar, F.J., 2010. Ecostratigraphic trends of Jurassic agglutinated foraminiferal assemblages as a response to sea-level changes in shelf deposits of Svalbard (Norway). Palaeogeography, Palaeoclimatology, Palaeoecology 293, 184—196.
Rogov, M.A., Shchepetova, E.V., Ippolitov, A.P., Seltser, V.B., Mironenko, A.A., Pokrovsky, B.G., Desai, B.G., 2019. Response of cephalopod communities on abrupt environmental changes during the early Aptian OAE1a in the Middle Russian Sea. Cretaceous Research 96, 227–240.
Roth, P.H., Bowdler, J., 1981. Middle Cretaceous nannoplankton biogeography and oceanography of the Atlantic Ocean. In: Warme, J.E., Douglas, R.G., Winterer, E.L. (Eds.), The Deep Sea Drilling Project: A Decade of Progress, vol. 32. SEPM. Special Publication, pp. 517–546.
Roth, P.H., Krumbach, K.P., 1986. Middle Cretaceous calcareous nannofossil biogeography and preservation in the Atlantic and Indian Oceans: implications for paleoceanography. Marine Micropaleontology 10, 235–266.
Sakharov, B.A., Lanson, B., 2013. X-ray identification of mixed-layer structures: modelling of diffraction effects. Developments in Clay Science 5, 51–135.
Savelieva, J.N., 2014. Palaeoecological analysis of Berriasian ostracods of the central Crimea. Volumina Jurassica XII (1), 163–174.
Schlanger, S.O., Jenkyns, H.C., 1976. Cretaceous oceanic anoxic events: causes and consequences. Geologie en Mijnbouw 55, 179–184.
Schornikov, E.I., 2005. The question of cosmopolitanism in the deep-sea ostracod fauna: the example of the genus Pedicythere. Hydrobiologia 538 (1–3), 193–215.

Schrank, E., 2010. Pollen and spores from the Tendaguru Beds, Upper Jurassic and Lower Cretaceous of southeast Tanzania: palynostratigraphical and paleoecological implications. Palynology 34 (1), 3–42. https://doi.org/10.1080/01916121003620106.

Shcherbinina, E., Gavrilov, Y., Iakovleva, A., Pokrovsky, B., Golovanova, O., Aleksandrova, G., 2016. Environmental dynamics during the Paleocene–Eocene thermal maximum (PETM) in the northeastern Peri-Tethys revealed by high-resolution micropalaeontological and geochemical studies of a Caucasian key section. Palaeogeography, Palaeoclimatology, Palaeoecology 456, 60–81.

Slater, S.M., Bown, P., Twitchett, R.J., Danise, S., Vajda, V., 2022. Global record of "ghost" nannofossils reveals plankton resilience to high CO2 and warming. Science 376 (6595), 853–856.

Sohn, I.G., 1961. Techniques for preparation and study of fossil ostracods. In: Moore, R.C. (Ed.), Treatise on Invertebrate Paleontology. Part Q, Arthropoda 3, Crustacea,Ostracoda. Geological Society of America and University of Kansas Press, N.Y., pp. 64–70

Spicer, R.A., Herman, A.B., 2010. The Late Cretaceous environment of the Arctic: a quantitative reassessment based on plant fossils. Palaeogeography, Palaeoclimatology, Palaeoecology 295 (3–4), 423–442.

Suchéras-Marx, B., Mattioli, E., Giraud, F., Escargue, G., 2015. Paleoenvironmental and paleobiological origins of coccolithophorid genus Watznaueria emergence during the Late Aalenian-Early Bajocian. Paleobiology 41 (3), 415–435.

Takashima, R., Nishi, H., Huber, B.T., Leckie, R.M., 2006. Greenhouse world and the Mesozoic ocean. Oceanography 19 (4), 64–74.

Tesakova, E.M., 2014. Jurassic Ostracodes of Russian Plate: Stratigraphy, Paleoecology and Paleogeography (Doctoral thesis). Geological Institute, Moscow, p. 455pp (in Russian).

Tissot, B.P., Welte, D.H., 1984. Petroleum Formation and Occurrence, second ed. Springer-Verlag, p. 538.

Trabucho-Alexandre, J., Hay, W.W., de Boer, P.L., 2012. Phanerozoic environments of black shale deposition and the Wilson cycle. Solid Earth 3, 29–42.

Traverse, A., 2007. Paleopalynology, second ed. Springer, Dordrecht, p. 813.

Tremolada, F., Erba, E., 2002. Morphometric analysis of the Aptian Rucinolithus terebrodentarius and Assipetra infracretacea nannoliths: implications for taxonomy, biostratigraphy and paleoceanography. Marine Micropaleontology 44, 77–92.

Tremolada, F., Erba, E., Bralower, T.J., 2006. Late Barremian to early Aptian calcareous nannofossil paleoceanography and paleoecology from the Ocean Drilling Program Hole 641C (Galicia Margin). Cretaceous Research 27, 887–897.

Tribovillard, N., Bout-Roumazeilles, V., Abraham, R., Ventalon, S., Delattre, M., Baudin, F., 2023. The contrasting origins of glauconite in the shallow marine environment highlight this mineral as a marker of paleoenvironmental conditions. Comptes Rendus Geoscience 355 (S2), 1–16.

Tyson, R.V., 1995. Abundance of organic matter in sediments: TOC, hydrodynamic equivalence, dilution and flux effects. In: Sedimentary Organic Matter: Organic Facies and Palynofacies. Springer Netherlands, Dordrecht, pp. 81–118.

Tyszka, J., 1994. Response of Middle Jurassic benthic foraminiferal morphogroups to dysoxic/anoxic conditions in the Pieniny Klippen Basin, Polish Carpathians. Palaeogeography, Palaeoclimatology, Palaeoecology 110 (1–2), 55–81.

Vakhrameev, V.A., 1991. Jurassic and Cretaceous Floras and Climates of the Earth. Cambridge University Press, Cambridge, UK, p. 318.

Van der Zwaan, G.J., Duijnstee, I.A.P., Den Dulk, M., Ernst, S.R., Jannink, N.T., Kouwenhoven, T.J., 1999. Benthic foraminifers: proxies or problem? A review of paleoecological concepts. Earth–Science Reviews 46, 213–236.

Voronova, M.A., 1984. Miospores of Lower Cretaceous of Ukraine. Naukova Dumka, Kiev, p. 118 (in Russian).

Voronova, M.A., Yanovskaya, G.G., 1991. Zones of vegetation cover of Jurassic and Early Cretaceous of Ukraine. Geological Journal 3, 72–81 (in Russian).

Weissert, H., Erba, E., 2004. Volcanism, CO_2 and palaeoclimate: a Late Jurassic–Early Cretaceous carbon and oxygen isotope record. Journal of the Geological Society 161 (4), 695–702. https://doi.org/10.1144/0016-764903-087.

Williams, G.L., 2003. Palynological analysis of Petro-Canada et al. Terra Nova K-18, Jeanne d'Arc Basin, Grand Banks of Newfoundland. Geological Survey of Canada, Open File 1659, 21p. https://doi.org/10.4095/214541.

Zakharov, Yu.D., Baraboshkin, E.Yu., Weissert, H., Michailova, I.A., Smyshlyaeva, O.P., Safronov, P.P., 2013. Late Barremian–early Aptian climate of the northern middle latitudes: stable isotope evidence from bivalve and cephalopod molluscs of the Russian Platform. Cretaceous Research 44, 183–201.

Zorina, S.O., 2014. Eustatic, tectonic, and climatic signatures in the lower Cretaceous siliciclastic succession on the Eastern Russian Platform. Palaeogeography, Palaeoclimatology, Palaeoecology 412, 91–98.

Zuo, F., Heimhofera, U., Hucka, S., T. Adatte, T., Erbacherc, J., Bodin, S., 2019. Climatic fluctuations and seasonality during the Kimmeridgian (Late Jurassic): stable isotope and clay mineralogical data from the Lower Saxony Basin, Northern Germany. Palaeogeography, Palaeoclimatology, Palaeoecology 517, 1–15. https://doi.org/10.1016/j.palaeo.2018.12.018.

Appendix

Table A.1
Values of the carbonate minerals in %.

Substage	CN zones	PF zones	Sample Nos	Carb, %
upper Aptian	NC7C	P. rohri	1	6.5
			2	3.9
			3	6.8
			4	5.3
			5	10.5
			6	11.4
		H. trocoidea	7	18.4
			8	18.7
			9	26.8
	NC7B	H. luterbacheri	10	22.3
			11	17.3
			1505	
	NC7A		1504	
			1503	
lower Aptian	NC6B	H. excelsa	13	5.3
			1502	
			1501	5.4
			14	5.4
			15	13.6
			16	18.8
	NC6A	*H. ruka* Bed	17	23.6
			18	25.0
		B. blowi	19	15.3
			20	28.0
upper Barremian			21	18.2
			22	20.4
			23	23.0

Table A.2
Pyrolysis Rock-Eval data for samples of the Upper Barremian–Aptian interval (the ZB section).

Substage	CN zones	PF zones	Sample nos	Sample weight, g	S0, mg HC/g rock	S1, mg HC/g rock	S2, mg HC/g rock	S3, mg CO/g rock	S0+S1+S2, mg HC/g rock	PI, Production Index, S1/S1+S2	*Tmax*, °C	TOC, wt%	HI, Hydrogen Index, S2/TOC*100	OI, Oxygen Index, S3/TOC*100
upper Aptian	NC7C	P. rohri	1	100.8	0	0.08	0.43	0.43	0.12	0.33	427	0.49	16	88
			2	96.6	0	0.09	0.32	0.32	0.13	0.31	437	0.74	12	43
			3	92.0	0	0.13	0.42	0.42	0.18	0.28		0.80	16	53
			4	89.8	0	0.07	0.45	0.45	0.12	0.42	434	0.72	10	63
			5	92.0	0	0.07	0.56	0.56	0.10	0.30	429	0.61	11	92
			6	87.8	0	0.06	0.81	0.81	0.12	0.50	475	0.68	9	119
		H. trocoidea	7	71.3	0	0.1	0.56	0.56	0.18	0.44	446	0.58	17	97
			8	81.0	0	0.07	0.59	0.59	0.10	0.30	416	0.44	16	134
			9	71.5	0	0.09	0.4	0.4	0.13	0.31	467	0.48	19	83
	NC7B	H. luterbacheri	10	73.4	0	0.12	0.49	0.49	0.18	0.33		0.54	22	91
			11	58.3	0	0.16	0.76	0.76	0.26	0.38		0.54	30	141
			1505	88.6	0.01	0.05	0.51	0.51	0.09	0.44	411	0.35	14	145
	NC7A		1504	71.0	0	0.13	0.74	0.74	0.17	0.24	430	0.38	34	195
			1503	67.7	0.01	0.12	0.83	0.83	0.19	0.37	416	0.46	26	180
lower Aptian	NC6B	H. excelsa	13	91.9	0	0.06	0.36	0.36	0.09	0.33	424	0.32	19	113
			1502	83.5	0.01	0.08	0.39	0.39	0.14	0.43	421	0.51	16	76
			1501	78.4	0	0.12	0.42	0.42	0.14	0.14	429	0.53	23	79
			14	90.6	0	0.41	0.34	0.34	0.50	0.18	429	0.65	63	52
			15	77.3	0	0.19	0.52	0.52	0.26	0.27	425	0.57	33	91
			16	75.1	0	0.21	0.72	0.72	0.42	0.50	493	0.40	53	180
	NC6A	H. ruka Bed	17	76.2	0	0.13	0.66	0.66	0.21	0.38		0.48	27	138
			18	86.2	0	0.1	0.51	0.51	0.18	0.44	488	0.39	26	131
		B. blowi	19	72.5	0.01	0.14	0.52	0.52	0.22	0.36	434	0.53	26	98
			20	88.8	0	0.28	0.31	0.31	0.45	0.38		0.43	65	72
U Barr.			21	85.0	0	0.09	0.47	0.47	0.12	0.25	420	0.45	20	104
			22	64.5	0.01	0.33	0.5	0.5	0.56	0.41		0.66	50	76
			23	76.3	0.02	0.05	0.46	0.46	0.11	0.55	417	0.53	9	87

Table A.3
$\delta^{13}C$ and $\delta^{18}O$ stable isotopes in ZB section.

Substage	CN zones	PF zones	Sample Nos	Dentalina spp.			Bulk		
				$\delta^{13}C$ VPDB	$\delta^{18}O$ SMOW	$\delta^{18}O$ VPDB	$\delta^{13}C$ VPDB	$\delta^{18}O$ SMOW	$\delta^{18}O$ VPDB
upper Aptian	NC7C	P. rohri	1						
			2						
			3						
			4						
			5	0.6	30.5	0.5	3.8	28.8	−1.2
			6	1.6	30.4	0.4	4.5	29.4	−0.6
		H. trocoidea	7	1.3	30.6	0.6	4.3	28.1	−1.9
			8	−1.4	25.2	−4.8	3	29.6	−0.4
			9	−1.6	27.4	−2.6	1.6	28.3	−1.7
	NC7B	H. luterbacheri	10	−1.8	25.5	−4.5	2	28	−2.0
			11	−1	26.2	−3.8	3.3	29.3	−0.7
			1505	0.8	28.7	−1.3	3.2	29	−1.0
	NC7A		1504	−5.4	26.5	−3.5	1.6	27.6	−2.4
			1503	−4.7	26.6	−3.4	0.2	27.3	−2.7
lower Aptian	NC6B	H. excelsa	13						
			1502						
			1501						
			14						
			15	−1.7	25.2	−4.8			
			16	−1.9	26.6	−3.4	1.6	27.7	−2.3
	NC6A	*H. ruka* Bed	17	−1.8	26.1	−3.9	1.2	27.7	−2.3
			18	−2.1	27	−3.0	1.3	27.8	−2.2
		B. blowi	19	−1.3	25.8	−4.2	1.9	26.9	−3.1
			20	−1.7	26.5	−3.5			
U Barr.			21	−1.4	25.5	−4.5	1.6	27.7	−2.3
			22	−1.6	25.6	−4.4	1.6	27.7	−2.3
			23				1.2	28	−2.0